CHEMOGENETIC INHIBITION OF THE INFERIOR COLLICULUS: EFFECTS ON ELECTROPHYSIOLOGY AND BEHAVIOR

by

Nanami Miyazaki

A Thesis

Submitted to the Faculty of Purdue University

In Partial Fulfillment of the Requirements for the degree of

Master of Science

Department of Biological Sciences

West Lafayette, Indiana

December 2018

THE PURDUE UNIVERSITY GRADUATE SCHOOL
STATEMENT OF COMMITTEE APPROVAL

Dr. Edward Bartlett

Department of Biological Sciences

Department of Biomedical Engineering

Dr. Susan Sangha

Department of Psychological Sciences

Dr. Esturado Robles

Department of Biological Sciences

Approved by:

Dr. Stephen Konieczny

Head of the Graduate Program

To my parents, siblings and close friends for their continuous support in my academic endeavors and career pursuit.

ACKNOWLEDGMENTS

I would like to thank Dr. Edward Bartlett for his mentorship throughout my master's career. Through his guidance, I was able to gain a multitude of research skills, insight on the field of auditory neuroscience and engage with diverse researchers within and outside of the Central Auditory Processing Lab. As such, I gained a rich research experience in a short two years which I believe will contribute greatly to my future academic endeavors.

I would also like to extend my gratitude to the past and present members of the Central Auditory Processing Lab, particularly Brandon Coventry, Alex Sommer, Marisa Dowling, Emily Han, Ryan Verner and Jesyin Lai. They provided much support throughout my master's career – whether it was training me on existing techniques, offering help on my project or sharing laughter in the lab – and made my experience at Purdue University a positive and unforgettable experience.

TABLE OF CONTENTS

TABLE OF CONTENTS 5
LIST OF FIGURES 7
ABBREVIATIONS 11
ABSTRACT 12
1. INTRODUCTION 13
2. ELECTROPHYSIOLOGICAL ASSESSMENT OF INFERIOR COLLICULUS CHEMOGENETIC INHIBITION 18
2.1 Methods 18
2.1.1 Subjects 18
2.1.2 Stereotaxic viral delivery 18
2.1.3 Auditory evoked potential recordings 19
2.1.4 Single-unit recordings 21
2.1.5 Acoustic stimuli 22
2.1.6 Analysis 23
2.2 Results 23
2.2.1 Auditory brainstem response recordings 23
2.2.2 Envelope following response recordings 26
2.2.3 Single-unit recordings 30
3. BEHAVIORAL ASSESSMENT OF INFERIOR COLLICULUS CHEMOGENETIC INHIBITION 20
3.1 Methods 20
3.1.1 Subjects 20
3.1.2 Acoustic startle response & prepulse inhibition 20
3.1.3 Analysis 22
3.2 Results 23
4. HISTOLOGICAL VERIFICATION OF DREADDS EXPRESSION 25
4.1 Methods and Analysis 25
4.2 Results 25
5. DISCUSSION 29

APPENDIX 34
REFERENCES 37

LIST OF FIGURES

Figure 1:1 Summary of central auditory pathway. (A) Ascending auditory pathway in the rat. (B) Descending auditory pathway in the rat. Areas of particular interest include cochlear nucleus (CN), ventral and dorsal nucleus of the lateral lemniscus (VNLL and DNLL, respectively), inferior colliculus (IC) and medial geniculate body (MGB). Figure adapted from Pickles (2015). 14

Figure 1:2 Approaches for stereotaxic delivery or transgenic expression of viral vectors for chemogenetics. (A) The use of transgenic rodent models or delivery of viral vectors with expression under a cell-type specific promoter allows for cell-type specific expression. However, the approach is limited in pathway specificity. (B) Dual injections with cre-recombinase dependent DREADDs expression and cre-recombinase allow for pathway specificity. (C) Pathway specificity can be achieved with the approach described in (A) if infusion of designer drug is infused locally to the area of interest. (D) Combinations of different DREADDs constructs can allow for multiplexed cell manipulation. 15

Figure 2:1 Schematic of stereotaxic viral delivery. Viral vectors containing the cre construct were injected into the ventral division of the MGB and viral vectors containing the DREADDs construct were injected into the central division of IC. The dual injection method allows for expression of the designer receptors specifically in the pathway between MGB and IC. Control animals received injections of AAV-CBA-GFP in both MGB and IC. All animals were bilaterally injected. 19

Figure 2:2 Characteristic ABR waveform and corresponding generators. Adapted figure [1]. .. 20

Figure 2:3 4-channel electrode configuration for auditory evoked potential recordings. 4 positive electrodes were placed along the sagittal suture (channel 1), the interaural line (channel 2), and the temporal ridge (channel 3 and 4). A ground electrode was placed along the nape of the neck and a negative electrode was placed along the mastoid. 21

Figure 2:4 Representative ABR waveforms from a single animal. Responses to sound levels ranging from 95-15 dB were collected for (A) channel 1, (B) channel 2, (C) channel 3 and (D) channel 4. 24

Figure 2:5 Averaged ABR waveforms from channel 1 for DREADDs animals (A-B) and control animals (C-D) before (A and C) and after (B and D) acoustic startle response training. Averages were compiled from 6 DREADDs and 2 control animals. Click stimuli were presented at 75dB. 25

Figure 2:6 Averaged ABR waveforms from channel 2 for DREADDs animals (A-B) and control animals (C-D) before and after acoustic startle response training. Averages were compiled from 6 DREADDs and 2 control animals. Click stimuli were presented at 75dB. 25

Figure 2:7 Averaged EFR spectrograms in response to IRN stimuli with 1000-500 Hz frequency sweep in DREADDs animals. Spectrograms represent responses before CNO administration before (A) and after (B) acoustic startle response training and after CNO administration before (C) and after (D) acoustic startle response training. (n=6). 26

Figure 2:8 Averaged EFR spectrograms in response to IRN stimuli with 1000-500 Hz frequency sweep in control animals. Spectrograms represent responses before CNO administration before (A) and after (B) acoustic startle response training and after CNO administration before (C) and after (D) acoustic startle response training. (n=2) 27

Figure 2:9 Averaged EFR spectrograms in response to IRN stimuli with 100-500 Hz frequency sweep in DREADDs animals. Spectrograms represent responses before CNO administration before (A) and after (B) acoustic startle response training and after CNO administration before (C) and after (D) acoustic startle response training. (n=6) 28

Figure 2:10 Averaged EFR spectrograms in response to IRN stimuli with 100-500 Hz frequency sweep in control animals. Spectrograms represent responses before CNO administration before (A) and after (B) acoustic startle response training and after CNO administration before (C) and after (D) acoustic startle response training. (n=2) 29

Figure 2:11 Average spiking rate in response to (A) BPN, (B) NAM, (C) IRN and (D) tone stimuli at time points after CNO administration. All spiking rates were normalized to the baseline spiking rate prior to CNO administration (0 min). Each animal's

recording was plotted individually in which red lines indicate DREADDs animals and black lines indicate control animals. Error bars represent standard deviations.. 31

Figure 2:12 Representative raster plots of single unit recordings of a DREADDs animal (A) and a control animal (B) in response to BPN stimuli. Raster plots represent distribution of neural activity firing before CNO administration (0 min) as well as 70 min and 110 minutes after CNO administration. Neural firing at stimuli (SGIs) of central frequencies ranging from 1-36kHz (numbered 1-22, respectively) are plotted against time (0.15-0.5 ms). Stimuli were presented from 0.2-0.4 ms, as indicated by the vertical lines on the plots. 32

Figure 3:1 Acoustic startle response and prepulse inhibition training paradigm. (A) The entire training paradigm lasted 8 days: 3 acclimation days and 3 test days. Each test day consisted of 3 blocks: acclimation, habituation and test session. (B) Each test session consisted of 9 blocks with 9 trials per block. In 1 trial, only the background tone. In 1 trial, both the background tone and prepulse were presented. In 1 trial, both the background tone and startle stimulus were presented. In 6 trials, background tone, prepulse tone and startle stimulus were presented and the interval between the beginning of the trial and the onset of the prepulse was varied. 21

Figure 3:2 Decrease in median maximum startle response over the course of 9 blocks in a single test session. Each bar represents the median startle response of all animals tested (DR01-DR05, DRC01, DRC03) for 3 test days. Error bars represent standard deviations..... 22

Figure 3:3 Median maximum startle responses and control condition responses of DREADDs (DR01-DR05) and control animals (DRC01, DRC03) over the course of 3 test days. For each animal, the left 3 bars represent maximum startle responses and the right 3 bars represent startle responses in control conditions in which only the background and prepulse tone is presented. All animals received an injection of CNO prior to the third test session. Error bars represent standard deviations..... 24

Figure 3:4 Median prepulse inhibition of DREADDs (DR01-DR05) and control animals (DRC01, DRC03) over the course of 3 test days. All animals received an injection of CNO prior to the third test session. Error bars represent standard deviations. No statistical significance was found using the Wilcoxon rank sums test. 24

Figure 4:1 Representative image of central IC of a DREADDs injected animal (DR03). GFP and mCherry expression are merged in the image. A vertical band of mCherry expression is observed along the center of the image while no GFP expression is observed in the image. 26

Figure 4:2 Representative image of central IC of a control animal (DRC03). GFP and mCherry expression are merged in the image. Relative spread of GFP expression is observed while no mCherry expression is observed in the image. 26

Figure 4:3 Relative optical density of central IC brain slices of all animals. All slices were imaged with excitation wavelengths of 395 nm and 587 nm corresponding to GFP and mCherry, respectively. The dotted line represents a relative optical density of 1 or no appreciable fluorescence compared to an unlabeled region. No GFP fluorescence was detected for DREADDs animals (DR01-DR06) while no mCherry fluorescence was detected for control animals (DRC03). 27

ABBREVIATIONS

ARHL	Age-related hearing loss
ASR	Acoustic startle response
BPN	Bandpass noise
CNO	Clozapine N-oxide
DREADDs	Designer receptors exclusively activated by designer drugs
EFR	Envelope following response
IC	Inferior colliculus
IRN	Iterated rippled noise
MGB	Medial geniculate body
NAM	Noise amplitude modulated
PPI	Prepulse inhibition
ROD	Relative optical density

ABSTRACT

Author: Miyazaki, Nanami L. MS
Institution: Purdue University
Degree Received: December 2018
Title: Chemogenetic Inhibition Of The Inferior Colliculus: Effects On Electrophysiology And Behavior
Major Professor: Edward Bartlett

Age-related hearing loss (ARHL) or presbycusis has grown to be a prevalent problem among the increasing aging population over the past century. Efficacy of hearing aids, cochlear implants or auditory brainstem implants have been shown, but with variable performance among patients, a fuller understanding of the complex circuitry of the auditory system would be beneficial for improving upon current technology as well as developing alternative treatments. In the current study, chemogenetics or DREADDs was utilized to inhibit the neuronal activity of the pathway between the medial geniculate body and the inferior colliculus. Subsequent effects of chemogenetic inhibition was assessed with electrophysiological measures– including auditory evoked potential recordings and single-unit recordings–as well as behavioral measures using the acoustic startle response and prepulse inhibition paradigm.

1. INTRODUCTION

The auditory pathway plays a critical role in processing the environment in addition to other sensory pathways such as the visual, olfactory, somatosensory and gustatory pathway. The following overview of the auditory pathway is adapted from Purves et al., 2012 [2]. Sound enters the auditory pathway as a pressure wave through the external ear, consisting of the pinna, concha and auditory meatus which direct the pressure wave to the tympanic membrane. The pressure is enhanced while traveling through the ossicles (malleus, incus and stapes) as it is transmitted from the large-diameter tympanic membrane to the small-diameter oval window of the cochlea. Through increased gain, the pressure wave is properly transmitted from the air into the cochlear fluid. The characteristic spiral shape and varied diameter of the cochlea allows for tonotopic organization in which lower frequencies resonate at the basal end of the basilar membrane and higher frequencies resonate the apical end. At the cochlea, the pressure wave is converted into neural signals through mechanical movement of the stereocilia of hair cells. The deflection of the stereocilia causes the opening cation channels which depolarize the hair cells. Subsequently, influx of calcium through voltage-gated calcium channels allows release of neurotransmitters from the hair cells to the auditory nerve.

Transmission continues through the auditory nerve which synapses onto the cochlear nuclei and diverges into pathways through the ipsilateral reticular formation or the contralateral superior olivary nucleus. Projections from these structures form the lateral lemniscus and converge onto the inferior colliculus (IC). Multiple converging inputs are integrated and modified in the IC to enable processing of complex temporal information. Signals continue to be transmitted to the medial geniculate body (MGB) in which additional integration and modification is conducted before reaching the auditory cortex.

Deficits or damage along the auditory pathway can manifest into hearing deficits. In particular, age-related hearing loss (ARHL) or presbycusis has grown to be a prevalent problem among the increasing aging population over the past century and is one of three major chronic conditions – along with hypertension and arthritis – to affect individuals above the age of 65 [3]. Current efforts to treat ARHL have included hearing aids and implants in the cochlea or auditory brainstem. Despite widespread use, these devices still pose issues for many patients. For instance, hearing aids lose their effectiveness in patients with severe hair cell damage and requires a relatively long

learning period to utilize the device to the fullest capacity [4]. Cochlear and auditory brainstem implants, on the other hand, have been more successful with widespread use but a high variability is observed between users [5].

The limitations in the current clinical approaches are likely attributed to the complexity of the auditory pathway, particularly in the central pathway. As seen in Figure 1, multiple projections to a region are common and decussations begin early within the ascending auditory pathway. Multiple projections and decussations are also seen in the descending auditory pathway, contributing to the complexity of the pathway [6]. Descending corticofugal projections have been implicated in plasticity of auditory structures in sound localization learning in ferrets [7] and in modulation of frequency maps in the IC of bats [8]. In addition to corticofugal projections, corticothalamic projections and feedback projections from the inferior colliculus to the super olivary nuclei have been observed in rats and have been suggested to be implicated in modulation of auditory processing as well as parallel processing of acoustic stimuli [9]. Along with the complexity of the auditory pathway, the molecular mechanisms of ARHL, whether it involves reduced mitochondrial function or changes in the physiological properties of the neurons, are still under investigation [10].

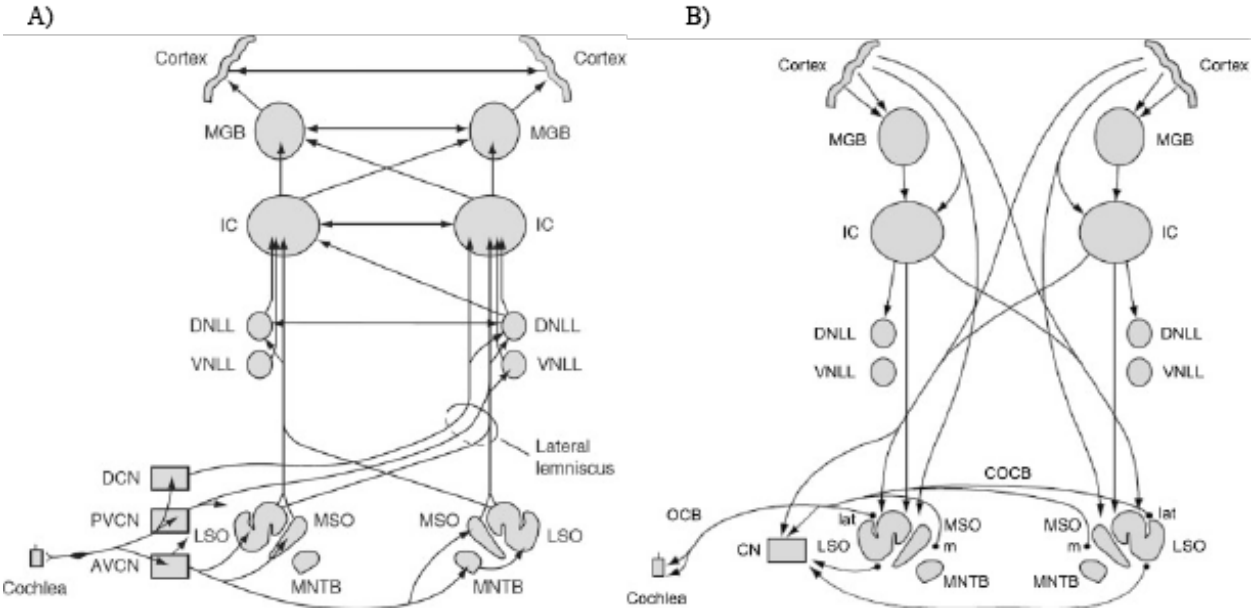

Figure 1:1 Summary of central auditory pathway. (A) Ascending auditory pathway in the rat. (B) Descending auditory pathway in the rat. Areas of particular interest include cochlear nucleus (CN), ventral and dorsal nucleus of the lateral lemniscus (VNLL and DNLL, respectively), inferior colliculus (IC) and medial geniculate body (MGB). Figure adapted from Pickles (2015).

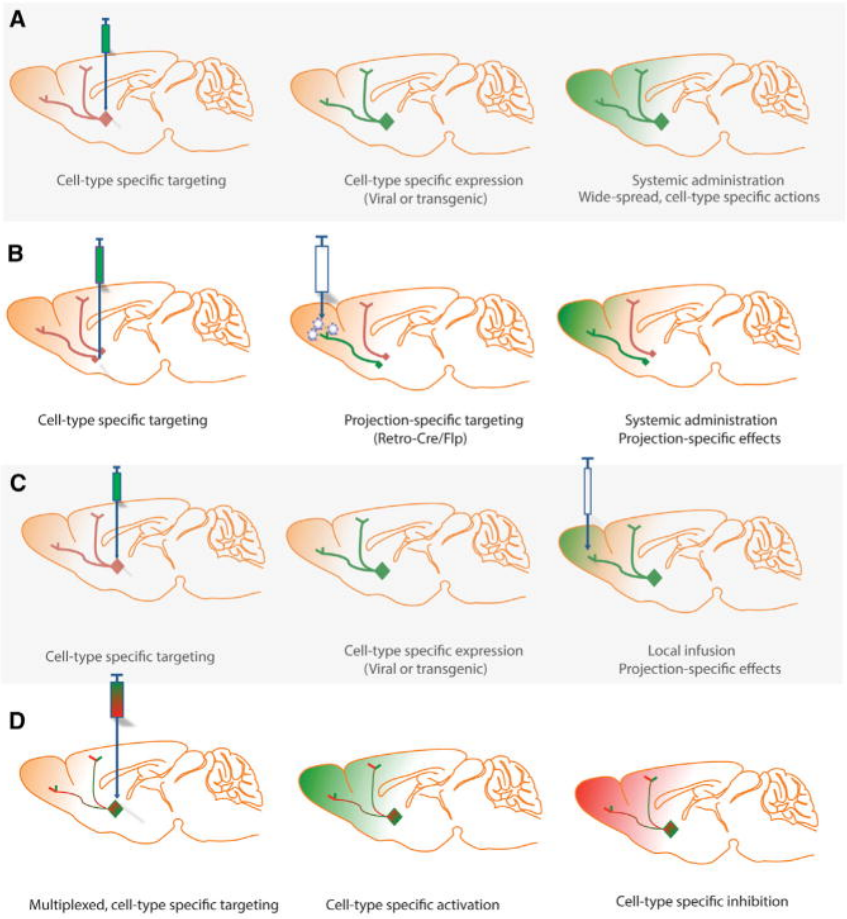

Figure 1:2 Approaches for stereotaxic delivery or transgenic expression of viral vectors for chemogenetics. (A) The use of transgenic rodent models or delivery of viral vectors with expression under a cell-type specific promoter allows for cell-type specific expression. However, the approach is limited in pathway specificity. (B) Dual injections with cre-recombinase dependent DREADDs expression and cre-recombinase allow for pathway specificity. (C) Pathway specificity can be achieved with the approach described in (A) if infusion of designer drug is infused locally to the area of interest. (D) Combinations of different DREADDs constructs can allow for multiplexed cell manipulation.

The focus of this study is the IC and MGB because previous studies have shown that auditory stimuli cannot bypass these structures in the ascending auditory pathway, that they are implicated in integration of spatial and temporal features and that they receive both ascending and feedback input from many areas along the pathway [6]. Current approaches to observe changes in the IC or MGB include immunohistochemistry of relevant proteins (e.g. GAD, vGluT2, vGlut1, $GABA_A$ receptors), non-invasive *in vivo* recordings (e.g. envelope following responses (EFR), frequency

following response (FFR) invasive single-unit or local field potential recordings [11]–[13] and pharmacological blockade of central auditory structures using drugs such as muscimol [14]. With the current approaches, however, it is difficult to target a specific pathway and determine a direct role in physiological or behavioral changes. Pharmacological blockade aims to determine a causative interaction but often lacks the ability to target particular projections.

Chemogenetics, or designer receptors exclusively activated by designer drugs (DREADDs), and optogenetics, however, offers the ability to manipulate neuronal activity with high specificity. Stereotaxic injections of viral vectors allow for expression of designer receptors or channelrhodopsins limited to the injection site [15–18]. There are several strategies for introducing the viral vector expression into the system as seen in Figure 2. Specificity can be achieved through cell type specific promoters or Cre-recombinase-dependent DREADDs expression [15–18]. After expression, DREADDs can be activated by an exogenous designer drug which is most commonly clozapine N-oxide (CNO). Plasma levels of CNO have been observed to peak at approximately 30 minutes, decline 2 hours following administration and have sustained behavioral effects up to 6 hours following administration [19, 20]. Although optogenetics enables manipulation of neuronal activity with high temporal fidelity and much shorter onset times (seconds to milliseconds), DREADDs is more conducive for studies in which sustained manipulation of neuronal activity is desired (hours) [17]. In addition, CNO can be administered through various routes including intraperitoneal injections or incorporation into the diet or water supply [17]. DREADDs are also easier to incorporate into deeper structures compared to optogenetics which are limited by the length of the fiber optic. Furthermore, DREADDs are arguably easier to incorporate into an animal model as it typically involves a single, minimally-invasive injection surgery whereas optogenetics requires injection of viral vectors and implantation of a fiber optic to deliver light stimulation.

Chemogenetics has been utilized in a variety of studies ranging from in vitro or in vivo electrophysiology to behavioral assays. Previous studies have correlated increased excitatory DREADDs expression levels with increased c-Fos protein, a marker of recent neuronal activity, expression and reported colocalization of DREADDs and c-Fos expression in dorsomedial prefrontal cortex, dorsal striatum, brainstem structures and in hypothalamus [21–23]. Furthermore, a recent publication reported a significant positive correlation between the percent of neurons transduced with the DREADDs constructs and performance on a behavioral task in rhesus monkeys, suggesting a strong relationship between DREADDs expression levels and behavioral

effects [24]. Such studies suggest that DREADDs expression levels can be correlated to changes in neuronal activity and in performance on behavioral tasks.

Despite widespread use of chemogenetics and optogenetics in studies involving other sensory pathways in addition to studies in learning and memory and addiction, literature searches suggested little use in regards to the auditory pathway [21, 25]. In the present study, DREADDs was utilized to inhibit the neuronal activity in the ascending projection from the central IC to the ventral division of the MGB. Subsequent effects of inhibition will be assessed with auditory brainstem responses (ABR), envelope following responses (EFR), single-unit responses and an acoustic startle response (ASR) and prepulse inhibition (PPI), which tests discrimination of auditory stimuli.

2. ELECTROPHYSIOLOGICAL ASSESSMENT OF INFERIOR COLLICULUS CHEMOGENETIC INHIBITION

2.1 Methods

2.1.1 Subjects

5 female Fischer-344 rats (3-4 months, 200-350g) and 3 male Fischer-344 rats (3-4 months, 250-450g) were used for this study (Taconic Biosciences). All animals were individually housed upon arrival and had ad libitum access to standard rodent chow and water. All protocols were approved by the Purdue Animal Care and Use Committee (PACUC 1111000167).

2.1.2 Stereotaxic viral delivery

The following HSV constructs were injected into rats that express the DREADDs construct: hEF1α-LS1L-hM4Di-IRES-mCherry and hEF1α-cre (MIT Vector Core) is injected into the inferior colliculus and medial geniculate body, respectively. The Adeno-associated virus (AAV), AAV-CBA-GFP (UNC Chapel Hill Vector Core), is injected into both sites for control rats.

Surgical procedures were adapted from Lowery and Majewska (2010) [26]. Following induction with isoflurane in air (4%), animals were positioned into a stereotaxic frame with its head fixed. Isoflurane in air (1.5-2%) was delivered through a nose cone throughout surgery to maintain the animal under the anesthetic plane. Heart rate and blood oxygenation was monitored with a pulse oximeter. Physiological body temperature was maintained with a water-circulating heating pad. Toe pinch reflex was assessed once an hour throughout surgery. If the reflex was present, isoflurane levels were increased until the reflex was no longer present.

An initial incision along the sagittal suture from 5 mm posterior to lambda and 5 mm anterior to bregma was made. Periosteal tissue was removed and coordinates were zeroed at bregma. Bilateral craniectomies over central inferior colliculus (-8.3 mm, ±1.8 mm) and ventral division of the medial geniculate body (-6 mm, ±3.5 mm). Viral vectors were loaded into 5µL glass Hamilton syringes using a microsyringe pump controller (World Precision Instruments). The glass microsyringe (Hamilton) was lowered along the dorsal-ventral axis into inferior colliculus (-4.6 mm) and medial geniculate body (-6 mm) at a rate of 1 mm/minute. 1 µL of viral vector was delivered to each site at a rate of 1 µL/10 minutes. Once infused, the syringe was left at the site for

an additional minute before removal. The incision was sealed with 6-0 silk sutures which were removed 7-10 days after surgery.

Animals were monitored each day for 3-5 days after each surgery. Recovery of lost weight was verified and meloxicam (1 mg/kg, s.q.) was administered for pain management.

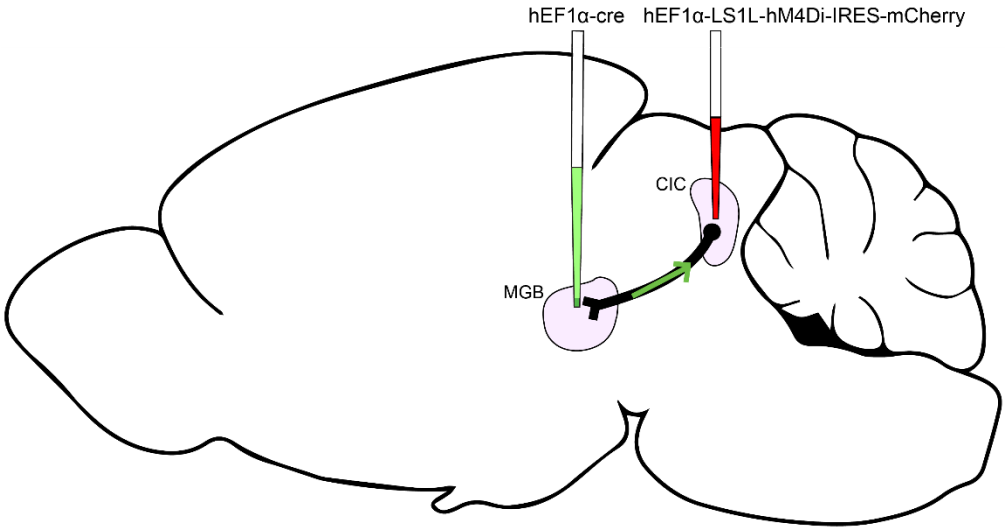

Figure 2:1 Schematic of stereotaxic viral delivery. Viral vectors containing the cre construct were injected into the ventral division of the MGB and viral vectors containing the DREADDs construct were injected into the central division of IC. The dual injection method allows for expression of the designer receptors specifically in the pathway between MGB and IC. Control animals received injections of AAV-CBA-GFP in both MGB and IC. All animals were bilaterally injected.

2.1.3 Auditory evoked potential recordings

Two types of auditory evoked potential (AEP) recordings were utilized for the present study: acoustic brainstem response (ABR) and envelope following response (EFR). As subdermal electrodes were utilized for the study, the ABR and EFR recordings can be regarded as auditory EEG signals. ABR waveforms capture the response of the auditory structures to click trains and are utilized to determine hearing thresholds[27, 28]. In addition, the ABR waveforms contains characteristic peaks which have been correlated to neural activity generated at different structures along the auditory pathway [28, 29]. As seen in Figure 2.2, Wave I-II correlates to activity from the cochlear nerve (CN), Wave III to the cochlear nuclei, Wave IV to the olivary nuclei and Wave V to the lateral lemniscus and IC [29]. EFR waveforms, on the other hand, utilize periodic or nearly periodic stimuli and represent the synchronized activity of populations of neurons [30]. In addition,

the response is unique in that the envelope of the response waveforms follows the envelope of the stimulus waveform with high fidelity [30].

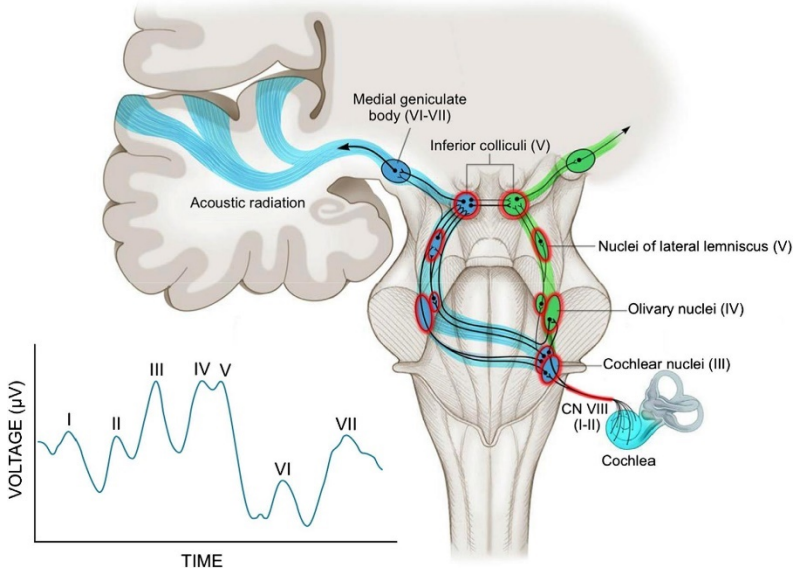

Figure 2:2 Characteristic ABR waveform and corresponding generators. Adapted figure [1].

AEP recording protocols described in previous publications were utilized [31, 32]. All recordings were performed in a 9’ x 9’ anechoic chamber (Industrial Acoustic Corporation). Following induction with isoflurane in air (4%), a lower concentration isoflurane in air (2%) was delivered through a nose cone while subdermal electrodes (Ambu) were placed into the scalp in a 4-channel configuration (Fig.2.3). For channel 1, a positive electrode was placed along the sagittal suture just caudal to the eyes. For channel 2, a positive electrode was placed along the interaural line. For channel 3 and 4, a positive electrode was placed parallel to channel 1 and along the temporal ridge of the ear ipsilateral and contralateral to the speaker, respectively. For all positive channels, the negative electrode was placed along the mastoid under the ipsilateral ear and the ground electrode was placed on the nape of the neck. Electrode impedance was checked using a low-impedance amplifier (RA4LI, TDT) and ensured to be less than 1 kΩ. Channel 1 has been reported to represent activity from caudal auditory brainstem structures while channel 2 was reported to represent activity from the lateral lemniscus and IC [32]. Channel 3 and 4 have not been characterized but are hypothesized to represent activity from lower auditory structures such as the auditory nerve. Further studies are needed to determine the generators for activity seen in channel 3 and 4.

Following electrode placement, animals were administered dexmedetomidine (Dexdomitor, 0.2 mg/kg, i.m.) and removed from isoflurane anesthesia to maintain the animal in a sedated state during the 2.5-3 hour recording sessions. Physiological body temperature was maintained with a water-circulating heating pad. All stimuli were presented via a farfield speaker placed 115cm from the animal. Stimuli were presented and responses were acquired using BioSig software (TDT).

CNO (3 mg/kg, i.p.) was administered after obtaining a single round of ABR and EFR responses. Prior to administration, isoflurane in air (2%) was delivered via a nose cone to minimize pain. After CNO was administered, the animals were taken off of isoflurane. Electrode positions were maintained before and after CNO administration. ABR and EFR responses were recorded once more 40 minutes after the CNO injection. AEP recordings were also collected before and after acoustic startle response and prepulse inhibition training.

Figure 2:3 4-channel electrode configuration for auditory evoked potential recordings. 4 positive electrodes were placed along the sagittal suture (channel 1), the interaural line (channel 2), and the temporal ridge (channel 3 and 4). A ground electrode was placed along the nape of the neck and a negative electrode was placed along the mastoid.

2.1.4 Single-unit recordings

Single-unit recording protocols described previously were utilized [33, 34]. Animals were administered ketamine (VetaKet, 60 mg/kg, i.m.) and dexmedetomidine (Dexdomitor, 0.15 mg/kg, i.m.) to achieve an anesthetic state. Heart rate and blood oxygenation was monitored with a pulse oximeter. Physiological body temperature was maintained with a water-circulating heating pad. Toe pinch reflex was assessed once an hour throughout surgery. If the reflex was present, supplemental doses of ketamine were administered intramuscularly.

An initial incision along the sagittal suture from 5 mm posterior to lambda and 5 mm anterior to bregma was made. Periosteal tissue was removed and a stainless steel headpost was adhered to the skull at bregma. The headpost was secured to the skull using three bone screws, one of which served as a ground screw, and dental cement (Dentsply). A 1-2 mm by 1-2 mm craniectomy centered on the previously made IC craniectomy was made.

Tungsten microelectrodes (A-M Systems, 2MΩ) encased in glass capillary tubes were advanced in the dorsal/ventral plane using a hydraulic microdrive (Narishige). Electrode outputs were sent through a headstage (RA4, TDT) and amplifier (RA4PA preamplifier, TDT) and recorded (RZ5, TDT) at a sampling rate of 24.42 kHz. Signals were filtered from 500 to 5000 Hz and spike-sorted using OpenEx and RPvdsEx software (TDT). Click stimuli were presented via a farfield speaker while advancing the electrode to find auditory-evoked responses. Once auditory-evoked responses were confirmed, responses to bandpass noise, noise amplitude modulated stimuli, iterated rippled noise and tuning were recorded prior to CNO (3 mg/kg, i.p.) injection. Recordings were resumed 10 minutes after CNO administration for 145-165 minutes after injection. At the conclusion of each acute recording, animals were euthanized with Beuthanasia (200 mg/kg) and transcardially perfused with phosphate buffer solution (PBS) and 4% paraformaldehyde.

2.1.5 Acoustic stimuli

The following stimuli were generated using SigGenRP (TDT): bandpass noise (BPN), click trains, noise amplitude modulated (NAM) stimuli and tones. Iterated rippled noise (IRN) stimuli were generated with custom-written MATLAB (Mathworks) software. IRN stimuli were generated from 250 ms white noise segments bandpass filtered from 80-32000 Hz with 32 iterations. Frequency sweeps of 100-500 Hz, 500-1000 Hz, 1000-500 Hz and 500-100Hz were applied to the IRN stimuli.

BPN, NAM, tones and IRN stimuli were utilized for single-unit recordings. For BPN stimuli, 22 signals of central frequencies ranging from 1-36 kHz were presented for a duration of 800 ms and 176 sweeps. For NAM stimuli, 9 signals of modulation frequencies ranging from 4-1024 Hz were presented for a duration of 2000 ms and 90 sweeps. IRN stimuli were presented for a duration of 2000 ms and 90 sweeps. Click stimuli and IRN stimuli were utilized to obtain ABR and EFR recordings, respectively, and presented at a 100-kHz sampling rate.

2.1.6 Analysis

ABR and EFR waveforms were high-pass filtered at 30 Hz and low-pass filtered at 3 kHz. ABR waveforms were separated by channel and compiled as an average waveform for comparison. Thresholds, indicated by the lowest sound level at which a response was present, were determined during each recording session before and after CNO administration. EFR responses from channel 1 were visualized as spectrograms which plot the frequency density over the course of each recoding window. The first 15 ms were excluded from spectrogram analysis as low frequency densities corresponding to ABR-like responses are present. IRN stimuli with frequency sweeps from 1000-500 Hz and 100-500 Hz were chosen for analysis as they were the stimuli utilized in the ASR and PPI paradigm.

Single-unit recordings were analyzed using custom-written MATLAB (Mathworks) software. Spiking rates for each signal was extracted and averaged for each type of stimuli (BPN, NAM, IRN and tones) and for each time point (0, 15, 20, 25, … 165 minutes). For single-unit responses, the Wilcoxon rank sum test was performed to compare average spiking rates at the time points after CNO administration to average spiking rates before CNO administration. Statistical significance was classified with a p-value of less than 0.05.

2.2 Results

2.2.1 Auditory brainstem response recordings

ABR waveforms were collected from the 4 channels, as seen in Figure 2.4, and utilized to determine the threshold of auditory perception. Thresholds for all animals ranged from 30-35 dB and was similar before and after acoustic startle training as well as before and after CNO administration (data not shown). Generally, the administration of CNO did not affect the amplitude of the overall waveform from channel 1 recordings in DREADDs animals (Fig.2.5a-b) or control animals (Fig.2.5a-b) at high sound levels tested. However, the waveform appears to have a latency shift with CNO administration in DREADDs animals (Fig.2.6a-b). The waveform appears to have a slight latency shift though not to the degree observed in DREADDs animals (Fig.2.6c-d). Similar trends were observed in channel 2 recordings in which waveform magnitudes were comparable before and after CNO administration and a slight latency was seen with CNO administration in all animals (Fig.2.7). Responses to lower sound level stimuli seemed to have change in the waveform

amplitude with CNO administration in all animals but is likely due to variability seen in responses at sound levels close to threshold as well as slight variability in thresholds (data not shown).

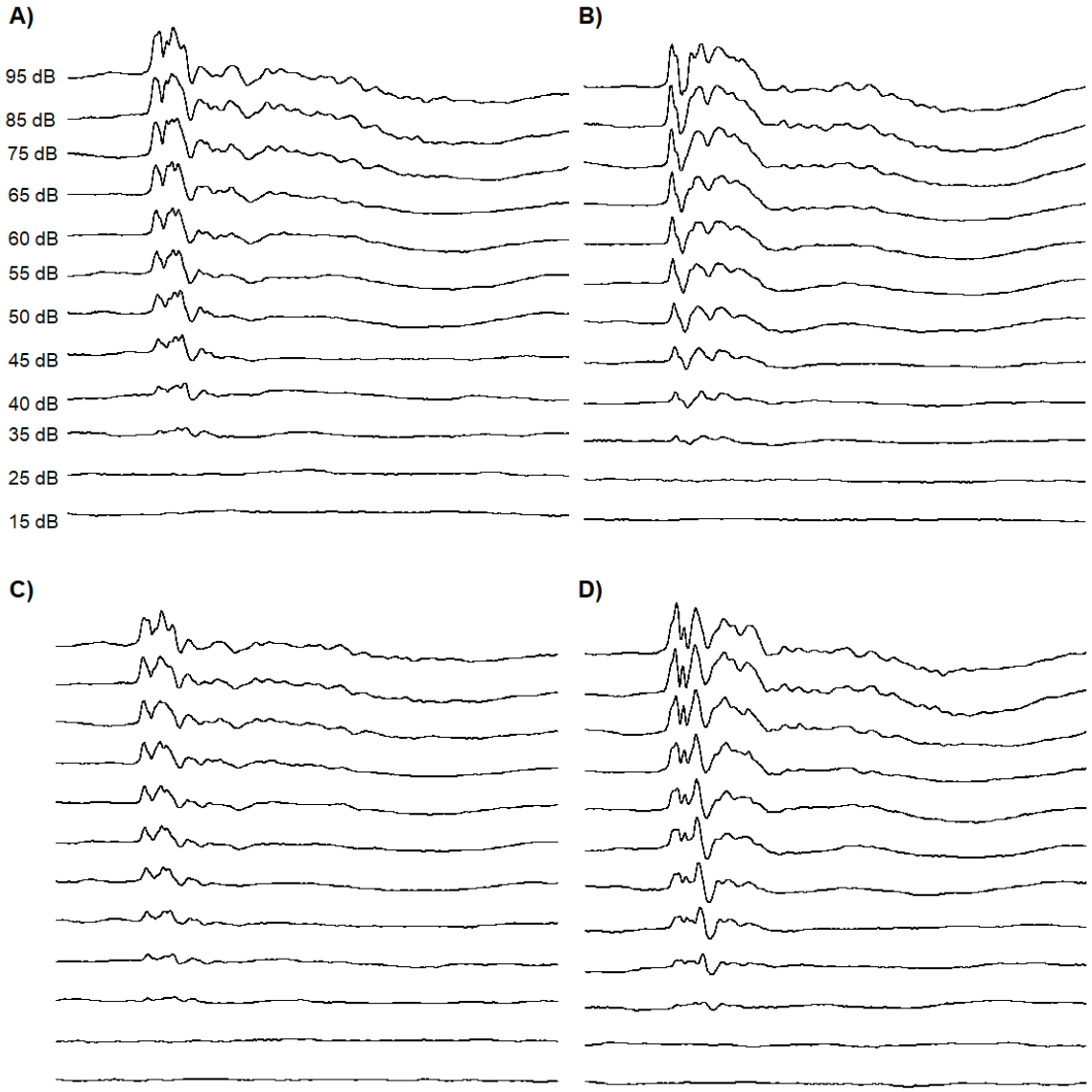

Figure 2:4 Representative ABR waveforms from a single animal. Responses to sound levels ranging from 95-15 dB were collected for (A) channel 1, (B) channel 2, (C) channel 3 and (D) channel 4.

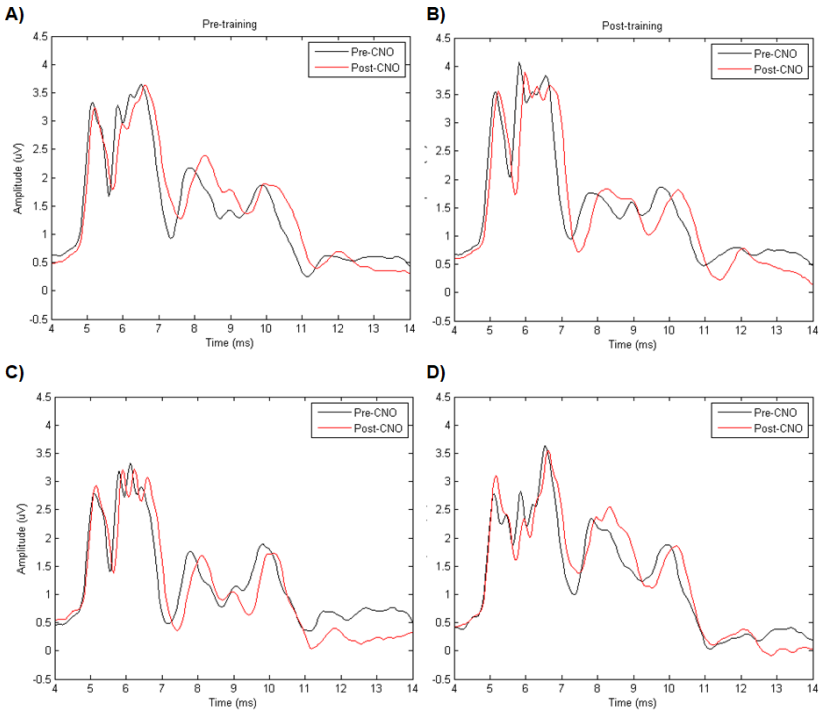

Figure 2:5 Averaged ABR waveforms from channel 1 for DREADDs animals (A-B) and control animals (C-D) before (A and C) and after (B and D) acoustic startle response training. Averages were compiled from 6 DREADDs and 2 control animals. Click stimuli were presented at 75dB.

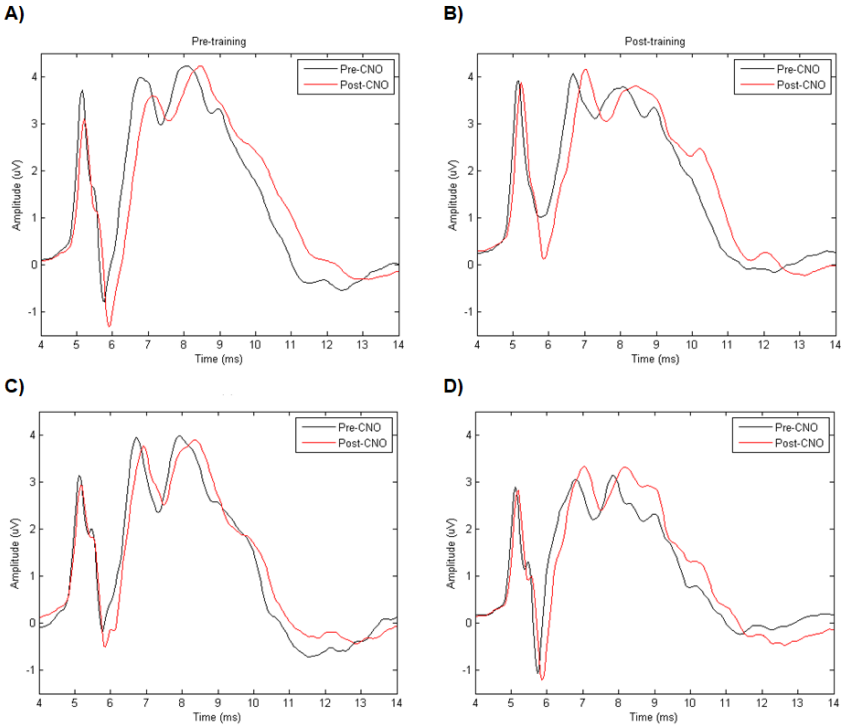

Figure 2:6 Averaged ABR waveforms from channel 2 for DREADDs animals (A-B) and control animals (C-D) before and after acoustic startle response training. Averages were compiled from 6 DREADDs and 2 control animals. Click stimuli were presented at 75dB.

2.2.2 Envelope following response recordings

Spectrogram analysis of DREADDs animals' responses to IRN tones with frequency sweeps from 1000-500 Hz suggest that there is a higher density of neural activity corresponding to this frequency sweep after ASR and PPI training as seen in the thinner bands of light blue and yellow which follow a linear stepwise trend from 1000-500 Hz (Fig.2.7a-b). This suggests that there is neural activity more confined to the frequency sweep following the acoustic discrimination learning task. With CNO administration before ASR and PPI training, the spread of neural activity density appears to decrease as reflected in smaller light blue bands (Fig.2.7c). After ASR and PPI training, the CNO appeared to have little effect on the spectrograms (Fig.2.7d).

Spectrogram analysis of control animals' responses to IRN tones with frequency sweeps from 1000-500 Hz also suggests similar neural activity locking to the stimuli. Neural activity is

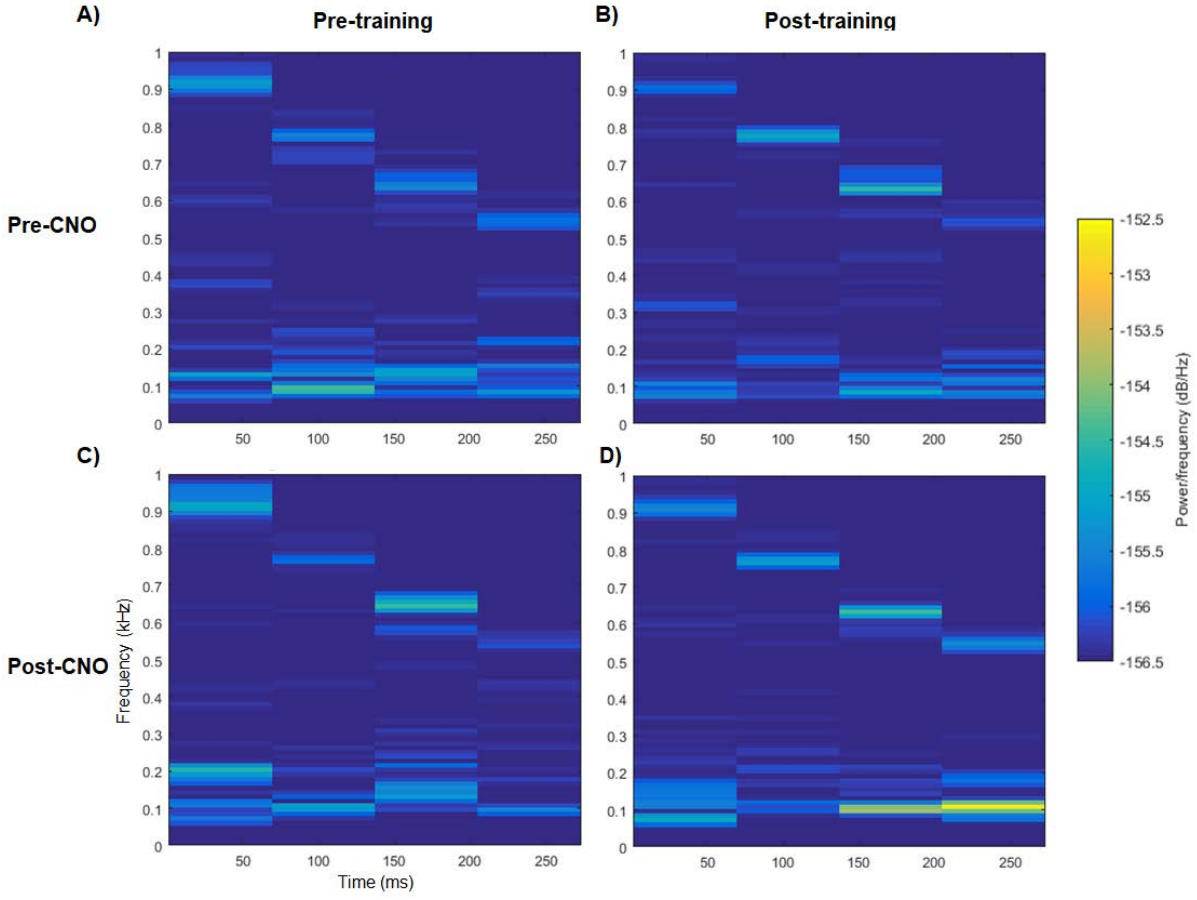

Figure 2:7 Averaged EFR spectrograms in response to IRN stimuli with 1000-500 Hz frequency sweep in DREADDs animals. Spectrograms represent responses before CNO administration before (A) and after (B) acoustic startle response training and after CNO administration before (C) and after (D) acoustic startle response training. (n=6).

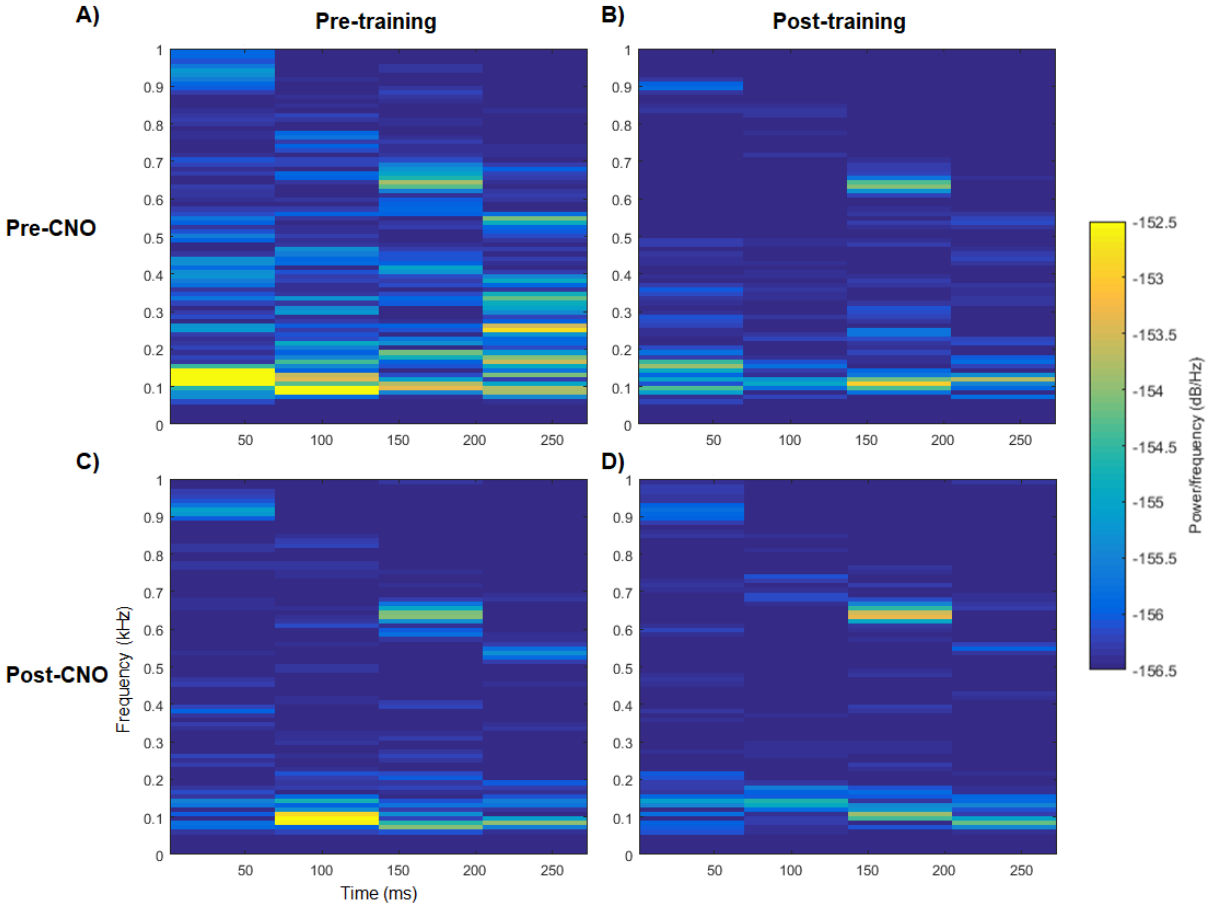

Figure 2:8 Averaged EFR spectrograms in response to IRN stimuli with 1000-500 Hz frequency sweep in control animals. Spectrograms represent responses before CNO administration before (A) and after (B) acoustic startle response training and after CNO administration before (C) and after (D) acoustic startle response training. (n=2)

spread across a wider range of frequencies before training in the control animals (Fig.2.8a) compared to DREADDs animals (Fig.2.7a). After ASR and PPI training, the density of neural activity appears to become more confined to the 1000-500 linear frequency range, suggesting increased ability to lock to the stimulus (Fig.2.8b). CNO administration appeared to decrease the spread of neural activity density before ASR and PPI training (Fig.2.8c), whereas it appeared to not change the density of neural activity considerably after ASR and PPI training (Fig.2.8d). While the effect seen after training is expected as CNO should be inert in control animals with no designer drug expression, the decreased activity observed before training was unexpected and might suggest

some baseline effects of CNO on wild-type animals. The relationship, however, is unclear due to a small sample size (n=2) and could benefit from the addition of more control animals to the study.

Spectrogram analysis of DREADDs animals' responses to IRN tones with frequency sweeps from 100-500 Hz, on the other hand, do not show frequency locking as clear as that seen with IRN tones with frequency sweeps from 1000-500 Hz. Locking to the 100-500 Hz linear frequency sweep can be observed before ASR and PPI training (Fig.2.9a) but appears to be obscured after ASR and PPI training by densities of neural activity which are spread over a larger frequency range (Fig.2.9b). The spread appears to be slightly mitigated with CNO administration as seen with the responses seen in Figure 2.7b (Fig.2.9d). Minimal effects, except for a slight increase in neural activity, were observed with CNO administration before ASR and PPI training (Fig.2.9c).

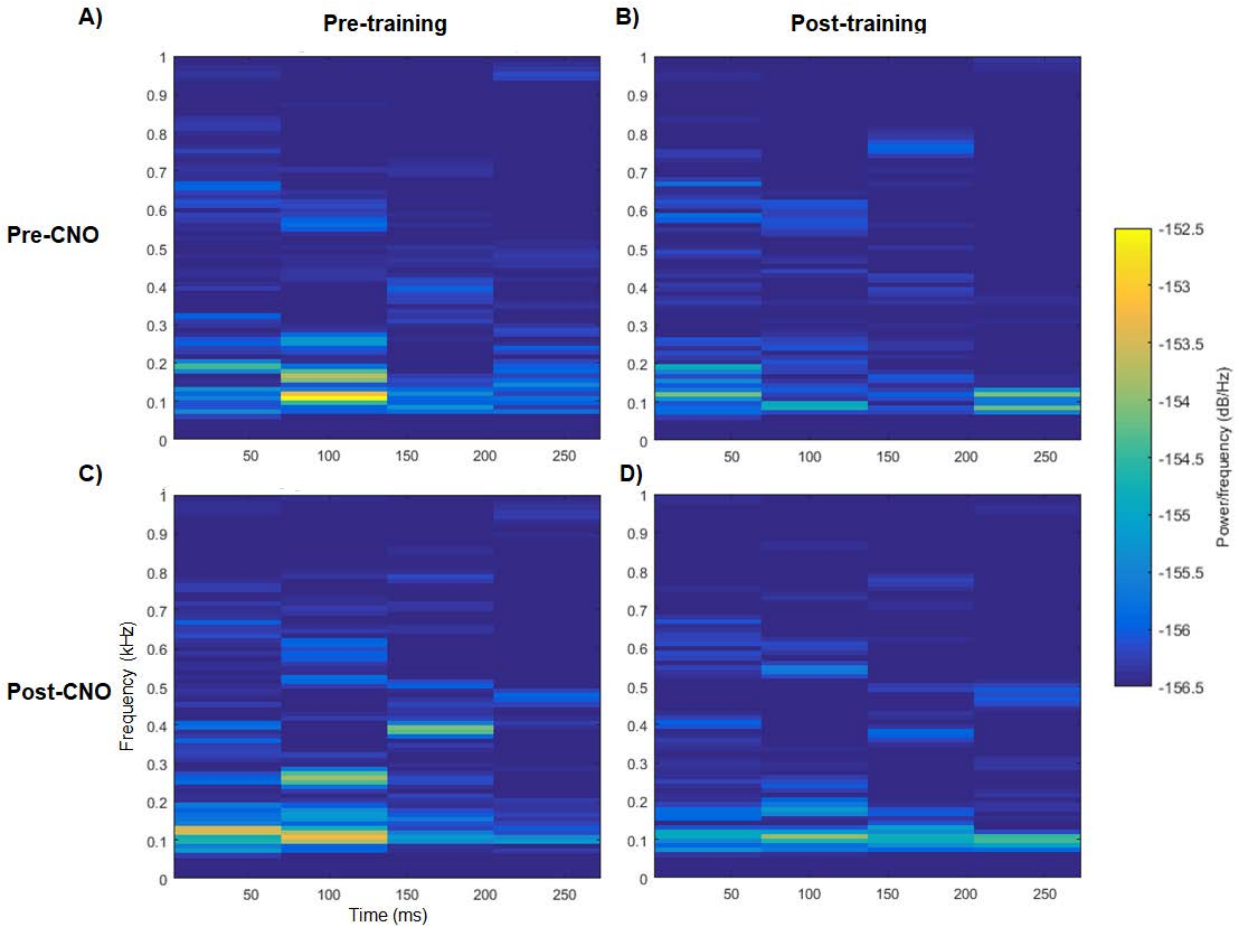

Figure 2:9 Averaged EFR spectrograms in response to IRN stimuli with 100-500 Hz frequency sweep in DREADDs animals. Spectrograms represent responses before CNO administration before (A) and after (B) acoustic startle response training and after CNO administration before (C) and after (D) acoustic startle response training. (n=6)

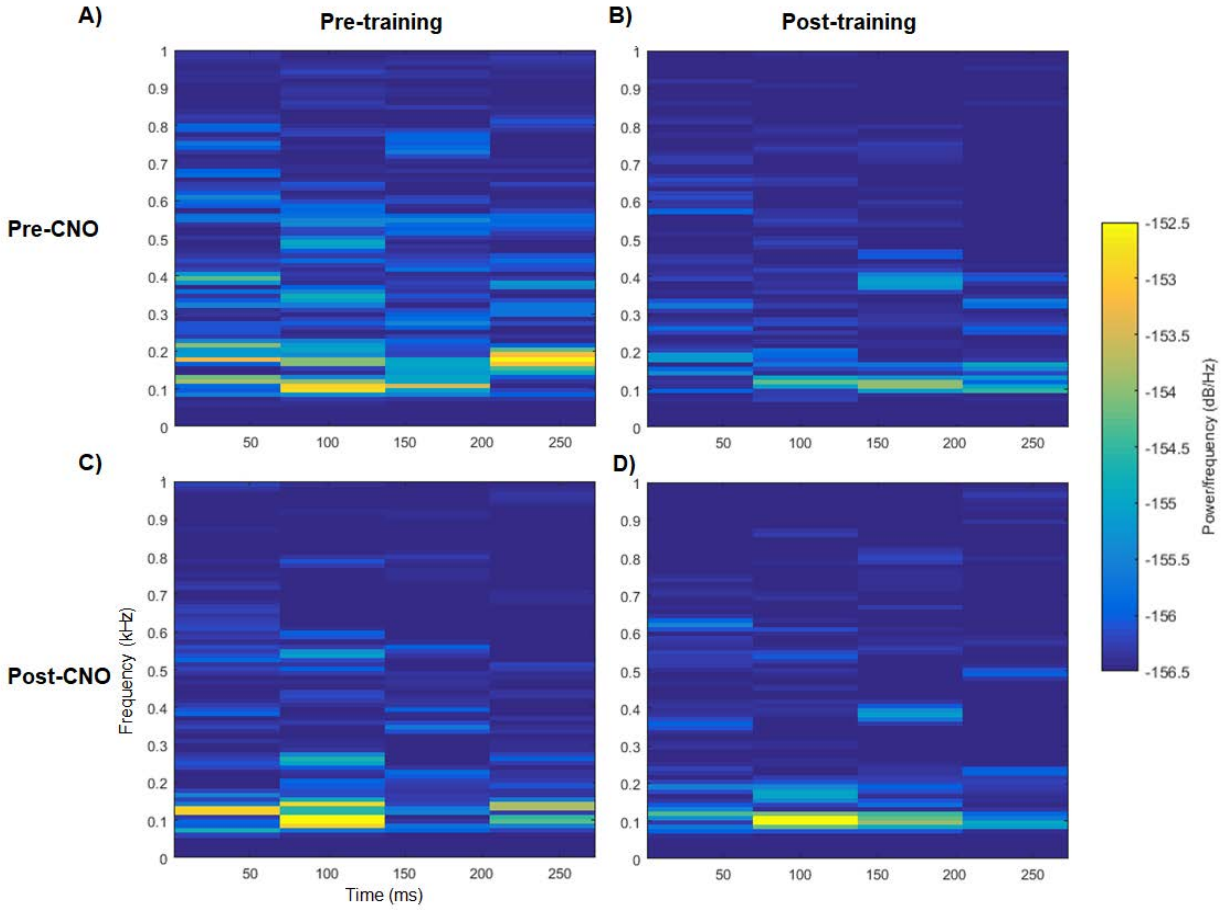

Figure 2:10 Averaged EFR spectrograms in response to IRN stimuli with 100-500 Hz frequency sweep in control animals. Spectrograms represent responses before CNO administration before (A) and after (B) acoustic startle response training and after CNO administration before (C) and after (D) acoustic startle response training. (n=2)

Similar to DREADDs animals, spectrogram analysis of control animals' responses did not display clear frequency sweep locking before (Fig.2.10a) and after (Fig.2.10), although the neural activity was confined to a small frequency range after ASR and PPI training. The minimized frequency range indicates an increased ability to lock to the stimulus, but the trend is not as clear as the one observed with responses to the IRN tone with frequency sweeps from 1000-500 Hz. With CNO administration, the overall spectrogram did not appear to change before (Fig.2.10c) or after (Fig.2.10d) ASR and PPI training, suggesting minimal effect of CNO on control animals with no designer receptor expression. Because effects were observed in control animals responding to IRN tone with frequency sweeps from 1000-500 Hz (Fig.2.8c), further investigation and a higher sample size would be beneficial.

Differences in the effects of CNO at the two different frequency sweeps observed may be attributed to frequency preferences in the central IC. A previous study reported that frequency following responses presented primarily monoaurally, similar to the experimental setup of the current study, were more present at low frequency stimuli and synchronization of neural activity decreases with increased stimulus frequency [35]. Based on these previous findings, the less pronounced effects with CNO administration with the IRN stimulus with the frequency sweep from 1000-500 Hz could be attributed to decreased neural synchronization or sensitivity to higher frequencies compared to the 100-500 Hz frequency sweep.

2.2.3 Single-unit recordings

Recordings from 3 animals (2 DREADDs and 1 control) were included in the analysis. The two DREADDs animals showed different trends following CNO administration. For animal DR02, the average spiking rate appeared to decrease for most time points. For animal DR05, the average spiking rate appeared to increase for most time points except for the responses to tones (Fig.2.11d). In addition, for animal DR02, the onset of the decreased activity agrees with previous studies which cite that effects of CNO were observed 20-30 min after adminstration [19]. Average spiking rates were signifcantly decreased compared to baseline levels with BPN, NAM and IRN stimuli at all time points for animal DR02 (Fig.2.11a-c). A general decrease in spiking activity was also observed with tone stimuli, but was found to be statistically signficant only at 65 and 85 min after CNO administration (Fig.2.11d). In addition, a recovery toward baseline levels was observed with BPN, IRN and tone stimuli beginning at 110 min, 120 min and 85 min after CNO administration, respectively. Previous literature suggest that the effects of CNO last around 2 hours, which appears to be consistent with the overall trends seen with DR02 [19]. A clear recovery was not observed with the NAM stimuli, but may be revealed with extended recording times. Representative raster plots of responses to BPN stimuli displays the decrease of neural firing 70 minutes after CNO administration (Fig.2.12a, middle row) compared to baseline levels (Fig.2.12a, top row) and a recovery toward baseline levels 100 minutes after CNO adminstration (Fig.2.12a, bottom row).

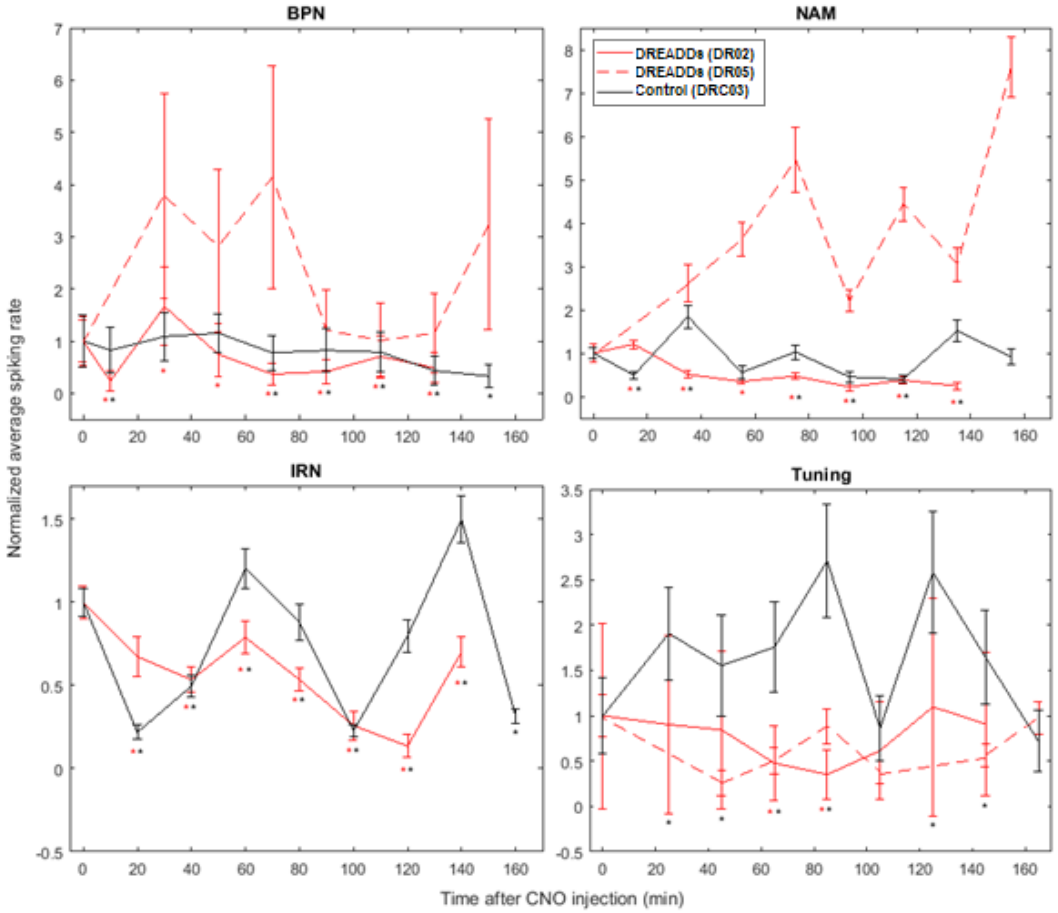

Figure 2:11 Average spiking rate in response to (A) BPN, (B) NAM, (C) IRN and (D) tone stimuli at time points after CNO administration. All spiking rates were normalized to the baseline spiking rate prior to CNO administration (0 min). Each animal's recording was plotted individually in which red lines indicate DREADDs animals and black lines indicate control animals. Error bars represent standard deviations.

Average spiking rates for the control animal oscillated around baseline levels with BPN, NAM and IRN stimuli (Fig.2.11a-c) but appeared to increase the average spiking rate for tone stimuli (Fig.2.11d). Statistically signifcant decreases were observed at several time points for BPN, NAM and IRN stimuli but tended to be less of a decrease than that of DR02 (Fig.2.11a-c). Representative raster plots of reponses to BPN stimuli displays a slight decrease in neural activity firing 70 minutes after CNO administration (Fig.2.12b, middle row) compared to baseline levels (Fig.2.12b, top row). The decrease in neural activity firing appears to be maintained at 100 minutes after CNO administration but not the the degree seen in the DREADDs animal.

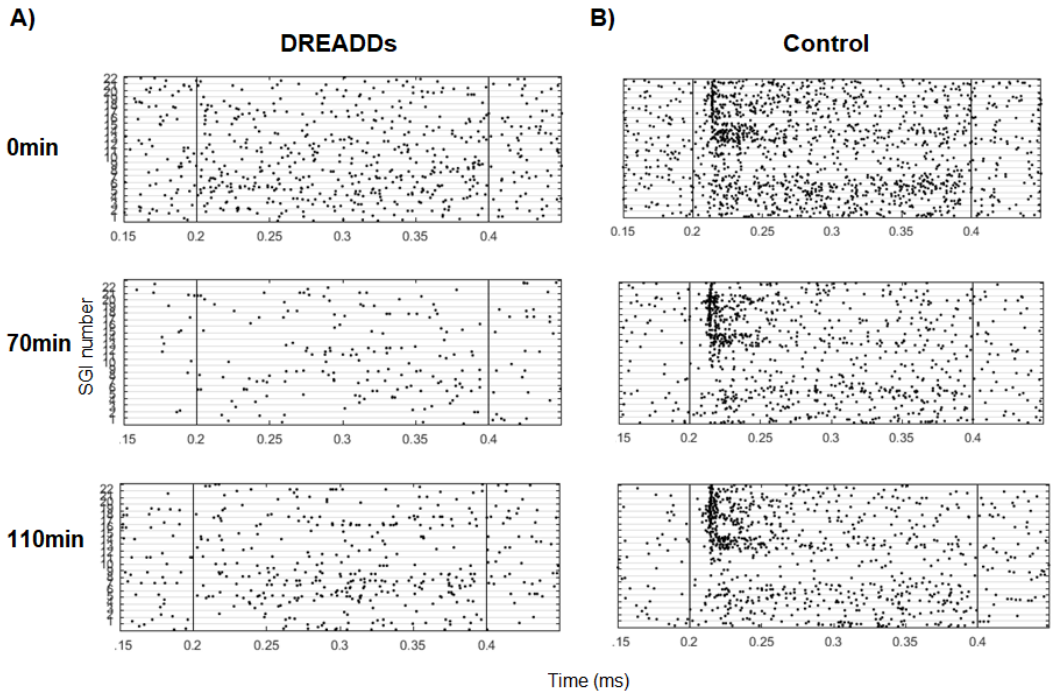

Figure 2:12 Representative raster plots of single unit recordings of a DREADDs animal (A) and a control animal (B) in response to BPN stimuli. Raster plots represent distribution of neural activity firing before CNO administration (0 min) as well as 70 min and 110 minutes after CNO administration. Neural firing at stimuli (SGIs) of central frequencies ranging from 1-36kHz (numbered 1-22, respectively) are plotted against time (0.15-0.5 ms). Stimuli were presented from 0.2-0.4 ms, as indicated by the vertical lines on the plots.

3. BEHAVIORAL ASSESSMENT OF INFERIOR COLLICULUS CHEMOGENETIC INHIBITION

3.1 Methods

3.1.1 Subjects

4 female Fischer-344 rats (3-4 months, 200-350g) and 3 male Fischer-344 rats (3-4 months, 250-450g) were used for this study (Taconic Biosciences). All animals were individually housed upon arrival and had ad libitum access to standard rodent chow and water. All protocols were approved by the Purdue Animal Care and Use Committee (PACUC 1111000167).

3.1.2 Acoustic startle response & prepulse inhibition

Figure 3.1 describes the ASR/PPI training protocols which were adapted from Floody and Kilgard (2007) and Valsamis and Schmid (2011) [36, 37]. Prior to ASR/PPI training, all animals were handled for three days. Animals underwent 3 consecutive days of acclimation (5 min, 7 min and 10min) to allow adaptation to the animal holder, startle box and the background noise. Following acclimation, the animals underwent 3 test days separated by 48 hours. Each test day consisted of a 5-min acclimation period, a 10-min habituation period (during which learning of the association between the prepulse and the subsequent startle stimulus occurred) and a 45-min test trial (Fig.3.1a). The 45-min test trial consisted of 9 blocks each with 9 trials (Fig.3.1b). For 6 trials, the interval between the beginning of the trial and the prepulse was varied and the startle stimulus was presented at a fixed interval after the prepulse. Three trials served as controls: For 1 trial, the prepulse was not presented, serving as a positive control. For 2 trials, only the background stimulus was presented, serving as a negative control. On the third test day, all animals were administered CNO (3 mg/kg, i.p.) 35 minutes before the beginning of the test session.

The IRN stimuli with frequency sweeps of 100-500 Hz and 1000-500 Hz were utilized as the prepulse and the background, respectively. White noise presented at 100 dB and for a duration of 20 ms was utilized as the startle stimulus. Background stimuli of 200 ms duration and interstimulus intervals of 100 ms were presented at 30 dB above threshold, which was determined through the ABR recordings previously obtained. The onset of the prepulse was varied between 15-30 s after the beginning of each trial. The interval between the prepulse and the startle stimulus was fixed at 50 ms for all trials. The startle response of the animal was measured through the

vertical movement of the platform which was transduced into a voltage signal and acquired with RZ6 Multi-I/O Processor (TDT).

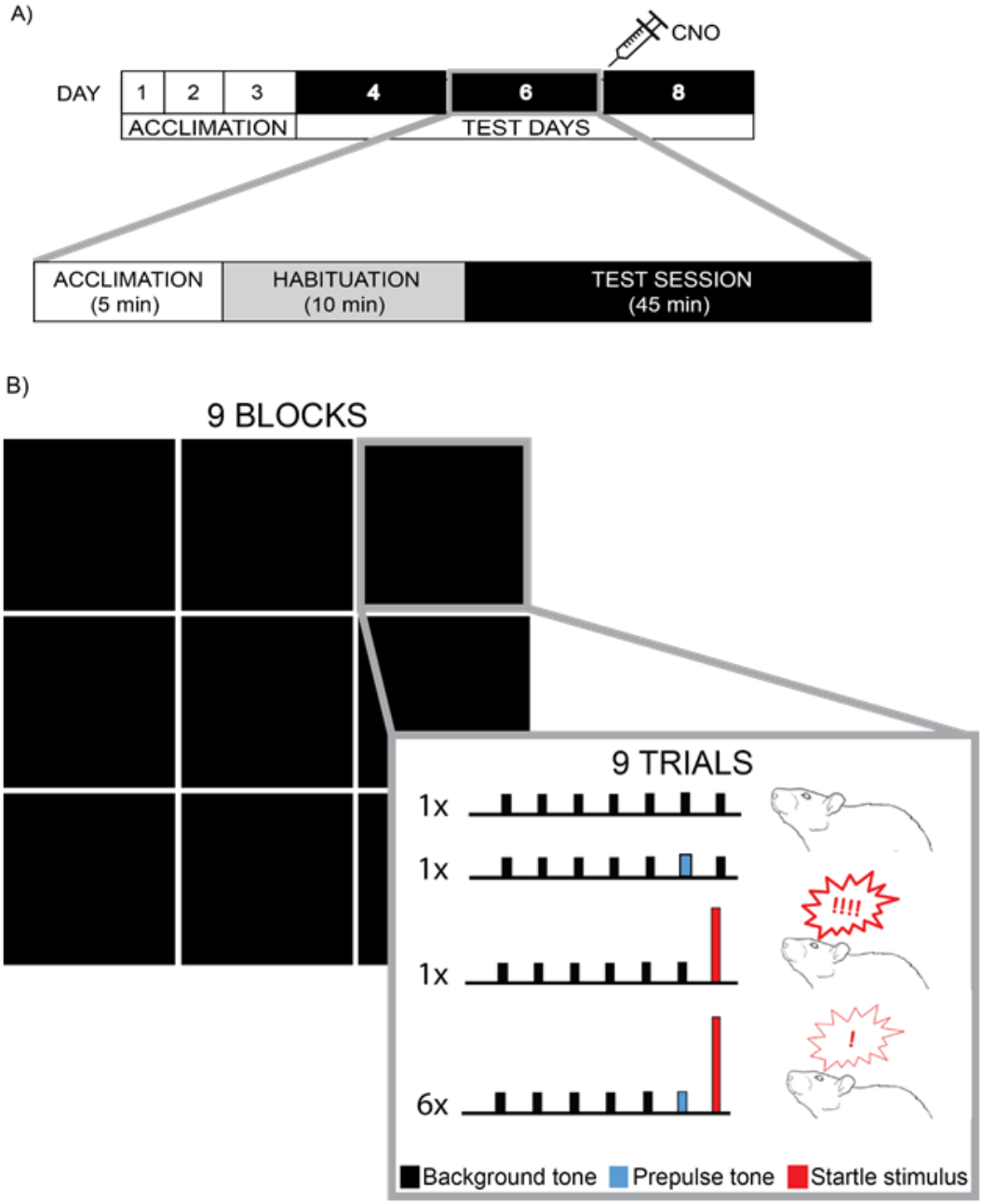

Figure 3:1 Acoustic startle response and prepulse inhibition training paradigm. (A) The entire training paradigm lasted 8 days: 3 acclimation days and 3 test days. Each test day consisted of 3 blocks: acclimation, habituation and test session. (B) Each test session consisted of 9 blocks with 9 trials per block. In 1 trial, only the background tone. In 1 trial, both the background tone and prepulse were presented. In 1 trial, both the background tone and startle stimulus were presented. In 6 trials, background tone, prepulse tone and startle stimulus were presented and the interval between the beginning of the trial and the onset of the prepulse was varied.

3.1.3 Analysis

Startle response was quantified using custom-written MATLAB (Mathworks) software. Responses from the first two blocks were utilized as habituation or a decline in maximum startle response was observed over the course of the 9 blocks in each animal as seen in Figure 3.2. In addition, the minimize variability, the maximum and minimum response of trials with background, prepulse and startle stimulus were excluded [38]. Prepulse inhibition trial responses were normalized to the maximum startle response in each trial (which consisted of only the startle stimulus and the background stimulus) and was represented as a percentage of the maximum startle response. A Wilcoxon rank sums test was performed to test statistical significance between startle responses across test days in one animal. Statistical significance was classified with a p-value of less than 0.05.

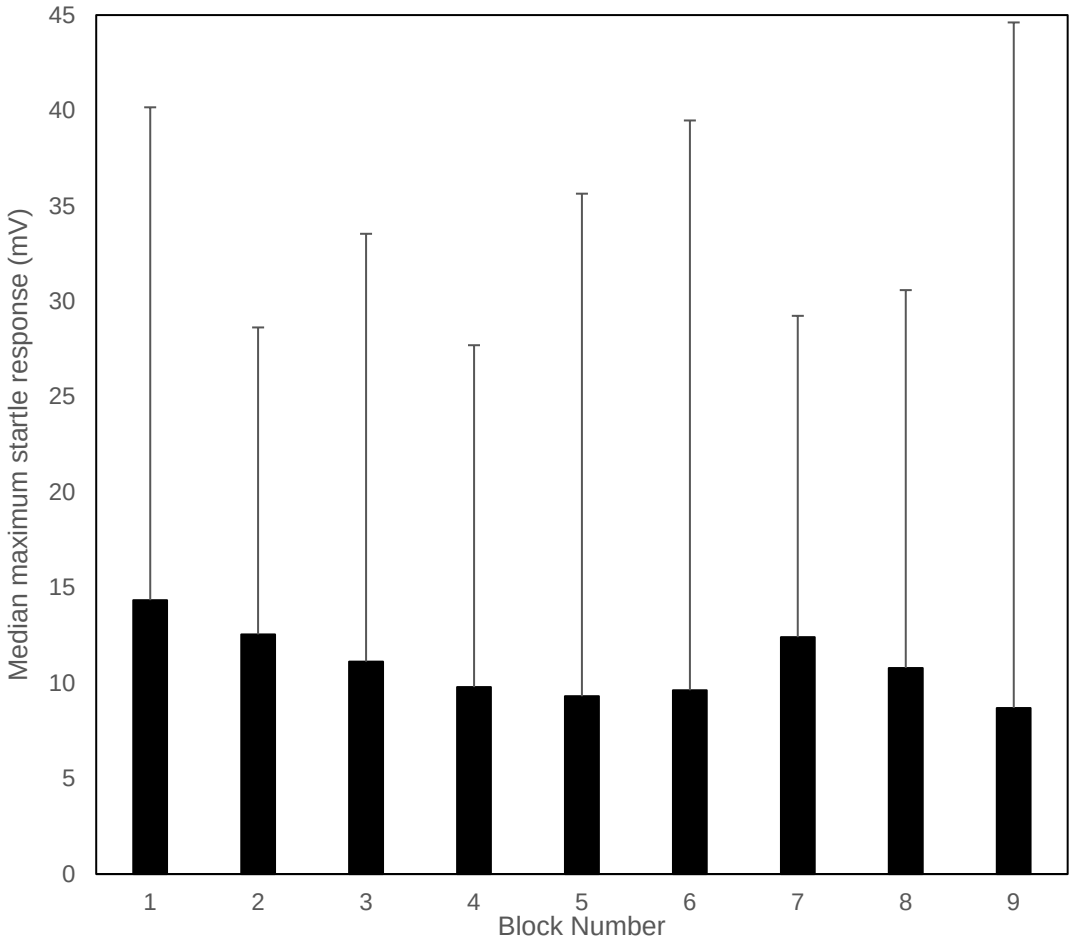

Figure 3:2 Decrease in median maximum startle response over the course of 9 blocks in a single test session. Each bar represents the median startle response of all animals tested (DR01-DR05, DRC01, DRC03) for 3 test days. Error bars represent standard deviations.

3.2 Results

As seen in Figure 3.3, fluctuation in the maximum startle response was observed in some animals, notably in animal DR01 and DR04 which both show decrease in maximum startle response over the course of 3 test days while animal DR03 shows an increase in maximum startle response. With the other animals tested, the maximum startle response remained relatively stable with high variability between animals (Fig.3.3). As seen in Figure 3.4, most animals were able to learn the association between the prepulse and the onset of the startle stimulus indicated by startle responses that were less than 100% of the maximum startle response during test days 1 and 2. Animal DR01, in particular, shows the predicted pattern in which the startle response was less than 100% of the maximum startle response on the first test day, further reduced on the second test day and rebounded or increased on the third test day during which CNO was administered (Fig.3.3). This trend suggests that inhibition of the IC appears to inhibit prepulse inhibition to a certain degree. As the ASR/PPI training serves as a test of auditory stimuli discrimination, the inhibition of IC may have impaired the ability of the DREADDs animals to discriminate between the prepulse and the background stimuli. A similar trend has been established in a previous study in which intraperitoneal injections of scopolamine, a muscarinic receptor antagonist, was found to inhibit prepulse inhibition compared to saline injections [39]. The trends, however, varied between the other DREADDs animals. When comparing the first and third test days, animal DR02 shows a similar inhibition of prepulse inhibition, but little change was observed in animal DR03 and a lack of inhibition was observed in animals DR04 and DR05. Control animals, on the other hand, did not have a noticeable rebound effect with CNO administration. Although a small rebound was seen in animal DRC01, the startle response amplitude continued to decrease compared to the first test day for DRC03. Thus, the results suggest that learning is not impaired with CNO in control animals. Changes in startle responses across test days for each animal was not found to be significant (p-value>0.05). The lack of statistical significance is likely due to the high variability within and between each animal. Statistical tests with the averaged responses of the 5 DREADDs animals or the 2 control animals also failed to yield statistical significance (p-value>0.05, data not shown). In addition, with the small number of animals included in the study, the statistical power of the study remains low for conclusive results

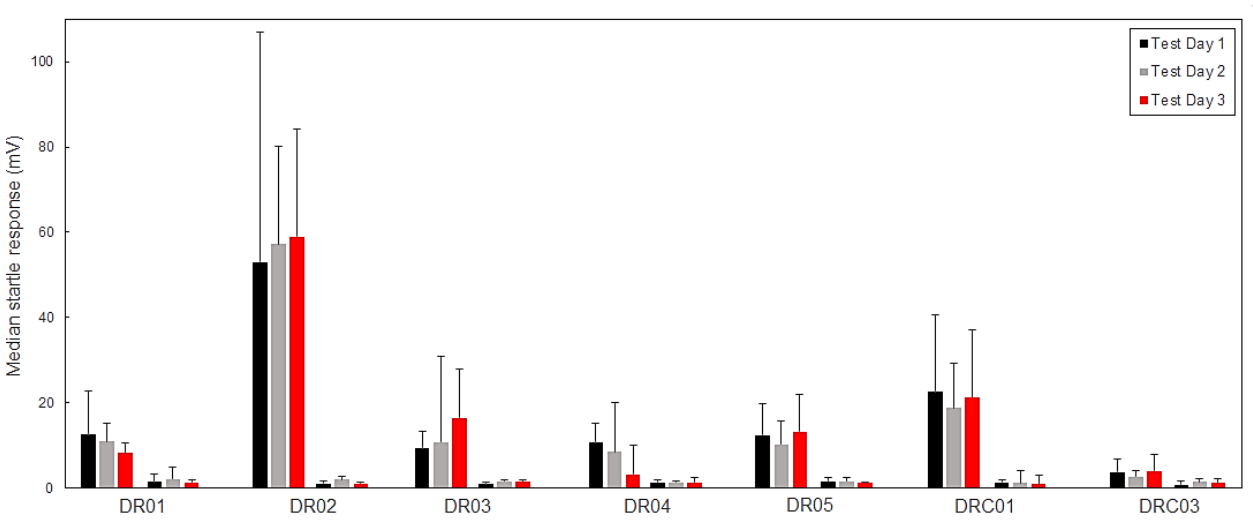

Figure 3:3 Median maximum startle responses and control condition responses of DREADDs (DR01-DR05) and control animals (DRC01, DRC03) over the course of 3 test days. For each animal, the left 3 bars represent maximum startle responses and the right 3 bars represent startle responses in control conditions in which only the background and prepulse tone is presented. All animals received an injection of CNO prior to the third test session. Error bars represent standard deviations.

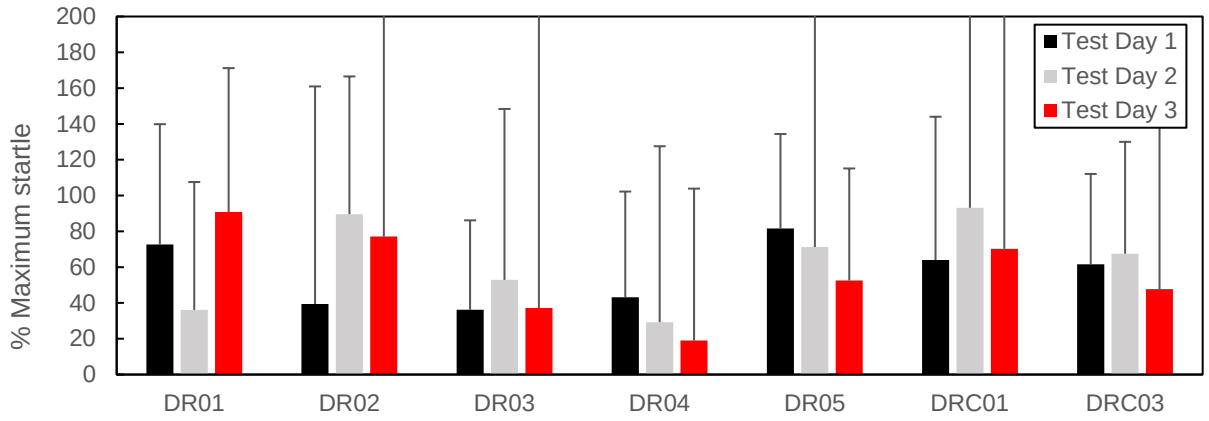

Figure 3:4 Median prepulse inhibition of DREADDs (DR01-DR05) and control animals (DRC01, DRC03) over the course of 3 test days. All animals received an injection of CNO prior to the third test session. Error bars represent standard deviations. No statistical significance was found using the Wilcoxon rank sums test.

4. HISTOLOGICAL VERIFICATION OF DREADDS EXPRESSION

4.1 Methods and Analysis

At the conclusion of single-unit recordings, all animals were transcardially perfused with 1M phosphate buffer solution (PBS) followed by 4% paraformaldehyde. Brains were extracted and incubated in 4% paraformaldehyde for 24 hours and transferred into 30% sucrose solution before freezing. 35µm slices were obtained using the Leica CM3050 Cryostat and mounted onto microscope slides using PBS and treated with Prolong Gold anti-fading reagent. Cover slips were sealed onto each slide using clear nail polish.

Slices were imaged under 10x magnification centered on central IC for image sizes of 849.8 µm2 using the Zeiss LSM 710 Confocal Microscope. The brightfield setting was utilized to locate the central IC with reference to the Rat Brain Atlas [40]. Tile scans of 2x1 images were taken and stitched together in Zen10 software. Excitation wavelength of 587 nm was utilized to capture mCherry fluorescence, which is included in the DREADDs vector, while an excitation wavelength of 395 nm was utilized to capture GFP fluorescence, which is included in the viral vector injected into control animals.

Relative optical density (ROD) measurements were obtained with ImageJ/Fiji software. ROD was calculated by normalized the average pixel intensity value of the region of interest with an unlabeled region. A ROD of 1 indicated the lack of fluorescence signals above background fluorescence while a ROD above 1 indicates fluorescence signals above background fluorescence.

4.2 Results

As seen in the representative image in Figure 4.1, mCherry expression but no GFP expression was observed in DREADDs injected animals (Fig.S1-S5). The opposite was observed in control animals in which GFP expression but no mCherry expression was observed (Fig.4.2) mCherry expression also appeared to be limited to small region compared to GFP expression which had more widespread expression. The differences in the localization of expression is likely due to the cre-dependent expression of the hEF1α-LS1L-hM4Di-IRES-mCherry viral vector which confines expression to the IC-MGB pathway in the present study. The AAV-CBA-GFP, however, is not cre-dependent and is more likely to spread from the injection site.

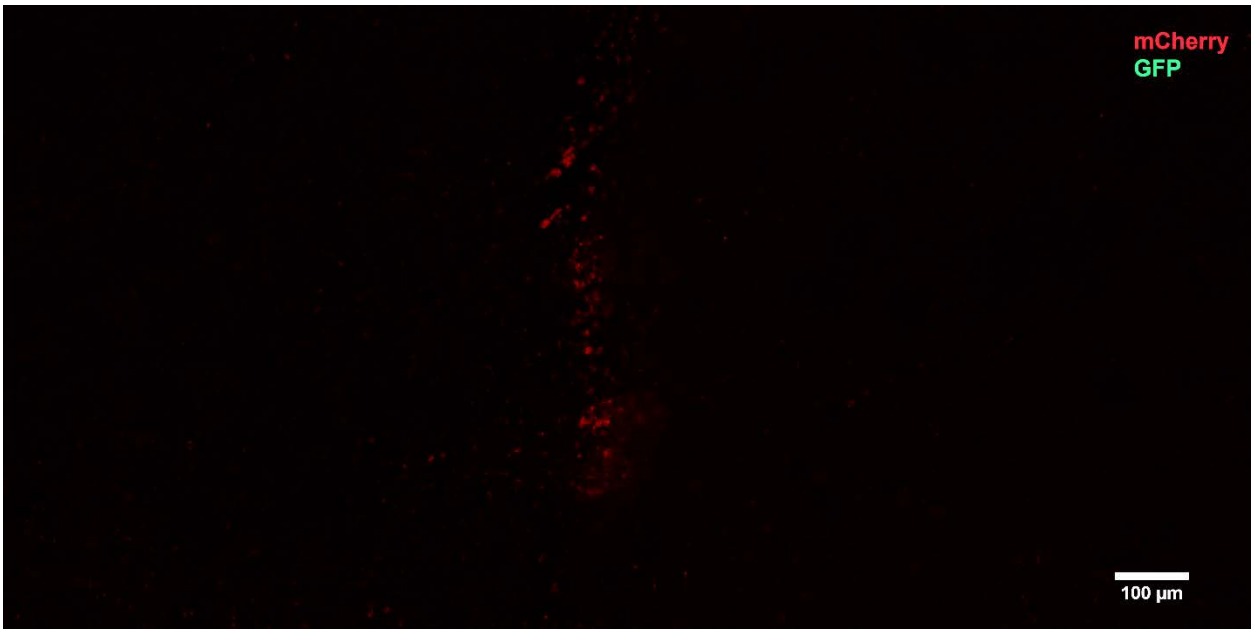

Figure 4:1 Representative image of central IC of a DREADDs injected animal (DR03). GFP and mCherry expression are merged in the image. A vertical band of mCherry expression is observed along the center of the image while no GFP expression is observed in the image.

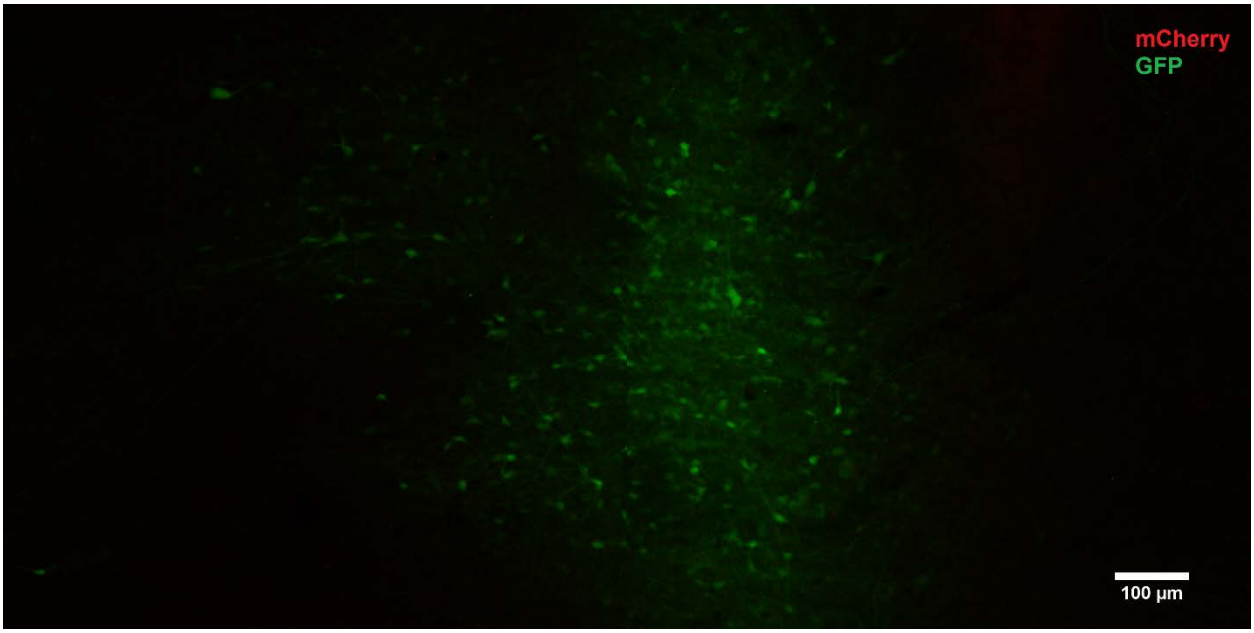

Figure 4:2 Representative image of central IC of a control animal (DRC03). GFP and mCherry expression are merged in the image. Relative spread of GFP expression is observed while no mCherry expression is observed in the image.

Expression levels of mCherry, quantified by ROD measurements, varied between all of the DREADDs animals, ranging from approximately 1.5-2 arbitrary units (Fig.4.3). Unexpectedly, ROD levels did not necessarily follow trends with ASR and PPI performance. For instance, animals DR01 and DR02 followed the expected trends of decreased prepulse inhibition with CNO administration (Fig.3.4) but did not have the highest ROD levels (Fig.4.3). Animal DR04, on the other hand, had comparable ROD levels but showed little effect of CNO on prepulse inhibition (Fig.3.4, Fig.4.3). Thus, improvements in quantification methods including averaging the ROD across multiple sequential slices may better capture the expression levels.

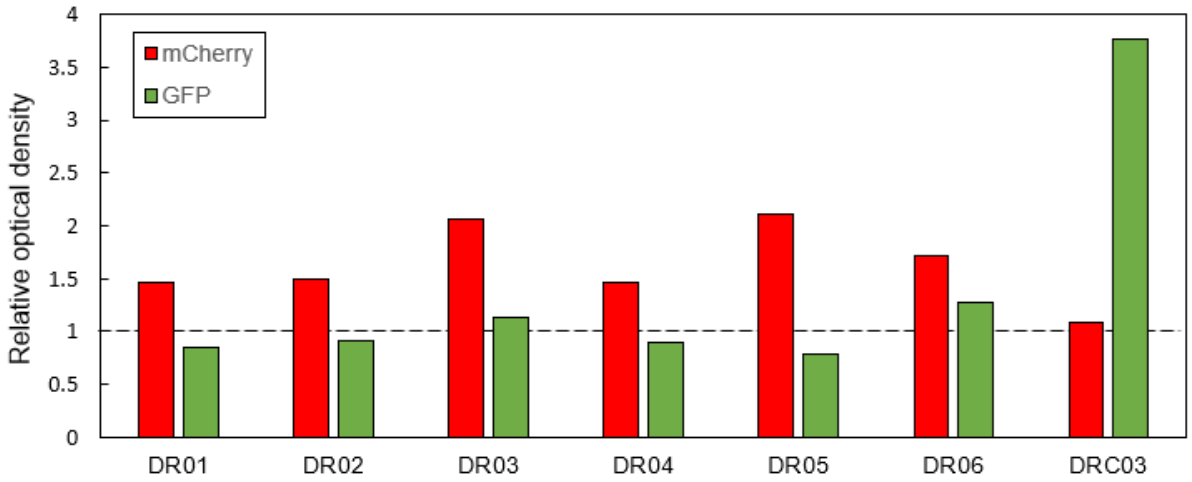

Figure 4:3 Relative optical density of central IC brain slices of all animals. All slices were imaged with excitation wavelengths of 395 nm and 587 nm corresponding to GFP and mCherry, respectively. The dotted line represents a relative optical density of 1 or no appreciable fluorescence compared to an unlabeled region. No GFP fluorescence was detected for DREADDs animals (DR01-DR06) while no mCherry fluorescence was detected for control animals (DRC03).

Notably, animal DR05 showed moderate mCherry expression levels but did not show any impact on prepulse inhibition with CNO administration (Fig.3.4). Histological assessment confirmed that the injection site was more rostral and lateral than the targeted site. Based on estimates from the Rat Brain Atlas, the injection site is estimated to be at the edge of the external cortex of the IC and the parasubiculum [40]. Because an auditory brain region was not likely expressing the designer receptor, the effects of CNO on prepulse inhibition was likely absent as seen in Figure 3.4. In addition, electrode track marks that were rostral and lateral to the central IC was observed in a few slices (data not shown). The location of the electrode tracks aligns with the

results seen with the single-unit recordings in which the trends of CNO administration on average spiking rate was nearly opposite to that of another DREADDs animal (Fig.2.7).

For control animal DRC03, high ROD levels of GFP were detected (Fig.4.3) which correlates to the widespread expression of GFP fluorescence observed in Figure 4.2. Fluorescence expression of GFP or mCherry was not observed in animal DRC01 (data not shown). The lack of fluorescence is likely due to the 7-month interval between the injection surgery and the perfusion of the animal. While the hEF1α-LS1L-hM4Di-IRES-mCherry vector allows for long-term fluorescence expression (MIT Vector Core), the AAV-CBA-GFP was not specifically indicated to have long-term fluorescence expression. Due to the prolonged period between the injection surgery and the perfusion, the fluorescence signal was likely degraded unlike animal DRC03 which had a shorter time interval between the injection surgery and the perfusion.

5. DISCUSSION

The current study suggests that chemogenetics could be a powerful tool for investigating the auditory system as effects were observed in single-unit responses, auditory evoked responses and performance on acoustic discrimination task. In general, chemogenetic inhibition of the central IC did not produce a notable change in hearing thresholds as the maximum increase in threshold with CNO administration observed in the current study was 5 dB. The overall shape of the ABR waveform was also unaffected with chemogenetic inhibition. The minimal effects observed align with previous studies which report that the auditory nerve is the primary generator of the ABR and lesions at auditory areas further along the auditory pathway produced changes at specific waves in the ABR waveform [28-29]. Because the current study selectively inhibited the central IC, there was likely compensation in the other structures along the auditory pathway which resulted in little changes observed in the threshold and the overall waveform. Further analysis of the ABR waveform could offer more insight into selective changes which result from the selective inhibition of the central IC. In particular, Wave V of the ABR waveform has been shown to correspond to IC activity [41]. Thus, comparing changes in the latency or the amplitude of Wave V with chemogenetic inhibition may reveal changes which are specific to the IC. Based on previous lesion studies, the magnitude of Wave V is predicted to decrease through not to the same degree as expression of the DREADDs was generally limited [29].

EFR recordings confirmed some changes in neural activity with ASR and PPI training, as increased ability to lock to the IRN stimuli frequency sweeps was observed after behavioral training. More pronounced effects observed at lower frequency stimuli may indicate sensitivity of the central IC to lower frequency stimuli compared to higher frequency stimuli. While CNO appeared to decrease neural activity for most DREADDs animals, there were variable effects which warrant further investigation and the addition of more animals to the study. Control animals, in general, did not have much change in the spectrograms, which suggests minimal or no effect of CNO on animals lacking designer receptor expression. However, there was an instance in which CNO appeared to decrease neural activity density in control animals in a recording session, suggesting a possibility of CNO affecting normal animals with no designer receptors. Again, with a small sample size, clear conclusions could not be drawn and a larger sample size is needed. Future studies would also benefit from additional analysis methods such as cross-correlation

analysis between the stimulus pitch contour and the response. Such analysis will facilitate quantification of frequency-locking to the frequency sweep in the IRN stimuli utilized. If the chemogenetic inhibition reduces frequency-locking responses, the cross-correlation values would be predicted to become close to zero.

Despite the variability in the single-unit responses, the inhibition of auditory evoked responses in IC with CNO administration was verified in one animal, showing promise of the technique for alternative studies. With a larger sample size, the effects of DREADDs inhibition would become more robustly supported. Through histological assessment, the unexpected trends observed in the single-unit recordings of the other DREADDs animal (DR05) was attributed to off-target injections and subsequent off-target electrode placement. Therefore, because the DREADDs was likely expressed in a non-auditory area, the responses to auditory stimuli were not inhibited as expected. CNO appeared to have some effect on the control animal, though arguably not to the degree seen in the DREADDs animal. Many recent publications have indicated the possible effects of CNO through accumulated levels of CNO through multiple injections or through reverse metabolism of CNO to clozapine [42–44]. While the single-unit recordings from this study might suggest a similar baseline effect, a larger sample size is needed for conclusive evidence. In addition, the current study may be improved by modifying the stimuli utilized. As seen in Figure 2.12, the responses in the DREADDs and control animal appeared to be more sensitive to higher frequency stimuli. Given the tonotopic organization of the IC, determining the central frequency of the recording site would be beneficial. Once the central frequency is determined, some stimuli can be presented at the frequencies which elicit the most response in a particular region. By presenting stimuli at the best frequency, the variability of the single-unit responses would likely be reduced and may provide a better comparison between animals. An additional electrode in auditory areas further along the auditory pathway than the IC or non-auditory regions would also provide insight into downstream effects of manipulation of the IC or provide a control condition to confirm changes specific to the auditory pathway, respectively. Alternatively, multi-channel electrodes which can record simultaneously at different depths of the IC could describe the spatial selectivity of the DREADDs.

The ASR and PPI results suggest some impairment of auditory stimuli discrimination as performance tended to worsen with the administration of CNO in some DREADDs animals, although this trend was not found to be statistically significant. The high variability observed in

the animals tested and could be improved by additional test days to obtain a more stable response prior to CNO administration or adjusting the interstimulus interval between the prepulse and startle stimulus. The current study utilized an interstimulus interval of 50 ms, but previous studies have shown successful prepulse inhibition with interstimulus intervals ranging from 5-500 ms in rats, suggesting potential in changing this interval [39]. In addition, habituation was observed over the course of the blocks in each test session, suggesting that experimental design of the startle training could be further improved by introducing additional discrimination tasks or decreasing the number of blocks to maintain the animal's attention and interest in the task. The protocol can also be extended to alternative stimuli to investigate different routes of auditory processing and the effects of manipulating the auditory structures involved such as detecting amplitude or frequency modulation changes in stimuli.

Histological assessment of the injection site for all animals confirmed expression of the DREADDs construct for all DREADDs animals and expression of GFP for one control animal. Expression in the central IC was confirmed in all animals except one which likely targeted a non-auditory area. Compared to the expression of GFP, the expression of DREADDs was relatively sparse which could explain the relatively minimal effects observed in the EFR waveforms and the variable effects observed in the ASR and PPI training. To combat sparse expression and reduce variability, future experiments could include multiple injections of the viral vectors to facilitate more robust expression of the DREADDs receptors throughout the central IC as opposed to a small region of IC. With more robust expression, the effects of chemogenetic manipulation is predicted to become more apparent in the EFR waveforms and ASR and PPI training. Single-unit recording trends would likely decrease in variability as well because electrode placement in an area with DREADDs expression would be easier with more widespread expression. Multiple injections would also be beneficial for manipulating neural activity larger auditory regions such as the auditory cortex which spans approximately 3 mm in the anterior-posterior plane [40]. The use of alternative viral vectors such as AAV vectors carrying the genetic information for DREADDs receptors may facilitate more widespread expression. For instance, AAV serotypes 2-5 were reported to have low expression, serotypes 1, 6 and 8 were reported to have moderate expression and serotypes 7 and 9 were reported to have high expression in mice [45]. As such, the use of an AAV7 or AAV9 vector which utilizes cre-dependent expression could ensure higher expression of the DREADDs while maintaining specificity to the IC-MGB pathway. The GFP expression in

the control animal was found to be much higher and widespread than the mCherry expression in DREADDs injected animals, likely due to the use of an AAV vector which did not have cre-dependent expression. As an additional control, future experiments could also include injections of GFP-expressing viral vectors which are also cre-dependent as further confirmation of the expression in the IC-MGB ascending pathway.

As the IC receives inputs from other auditory brain areas, future studies may also observe chemogenetic manipulation in alternative pathways. For instance, corticofugal projections that terminate onto nucleus of the brachium of the IC and the medial geniculate body have been confirmed with histological studies and have been suggested to play a role in cortical modulation of auditory processing [46]. Studies utilizing chemogenetic manipulation could supplement previous histological studies to determine the function of specific projections at different levels of auditory processing, ranging from the activity of a single neuron or behavior. Extending the study to utilizing cell-type specific DREADDs vectors could also be beneficial to isolate the effects of manipulating excitatory and inhibitory projections which have been implicated in a number of projections along the auditory pathway [7, 9]. A previous study demonstrated the utility of cell-type specific promoters in optogenetic silencing of excitatory neurons in the auditory cortex [47]. Based on the strong GABAergic projections from the central IC to the MGB previously reported in cats and rat, the use of viral vectors with promoters specific to GABAergic neurons may be useful to better target the IC-MGB projection to extend the current study [48–50]. As optogenetics and chemogenetics both utilize viral vectors with customizable promoters, cell-type specific promoters are feasible for future studies.

Developments in DREADDs technology have improved the utility of chemogenetics for a variety of applications. In addition to the commonly used CNO-activated designer receptors, the κ-opioid receptor has been engineered to create the κ-opiod receptor DREADD (KORD), which is activated by salvinorin B and is activated more rapidly than the stereotypical DREADDs [51]. Because the KORD construct is activated by a different designer drug, there is opportunity for multiplexed manipulation of neural activity. As both excitatory and inhibitory inputs from the central IC to the ventral division of MGB have been reported, the use of both salvinorin B and CNO-activated DREADDs may be beneficial for investigating effects manipulating each type of projection separately and in a reversible manner in the same animal [52]. Developments in making DREADDs technology more translatable have also been made ranging from bypassing invasive

intracranial injections with ultrasound-activated DREADDs expression (acoustically targeted chemogenetics) or the delivery of designer drugs with eye drops instead of an intraperitoneal injection [53, 54]. Such developments suggest some potential of utilizing DREADDs for clinical use with further development and refinement of the technique.

APPENDIX

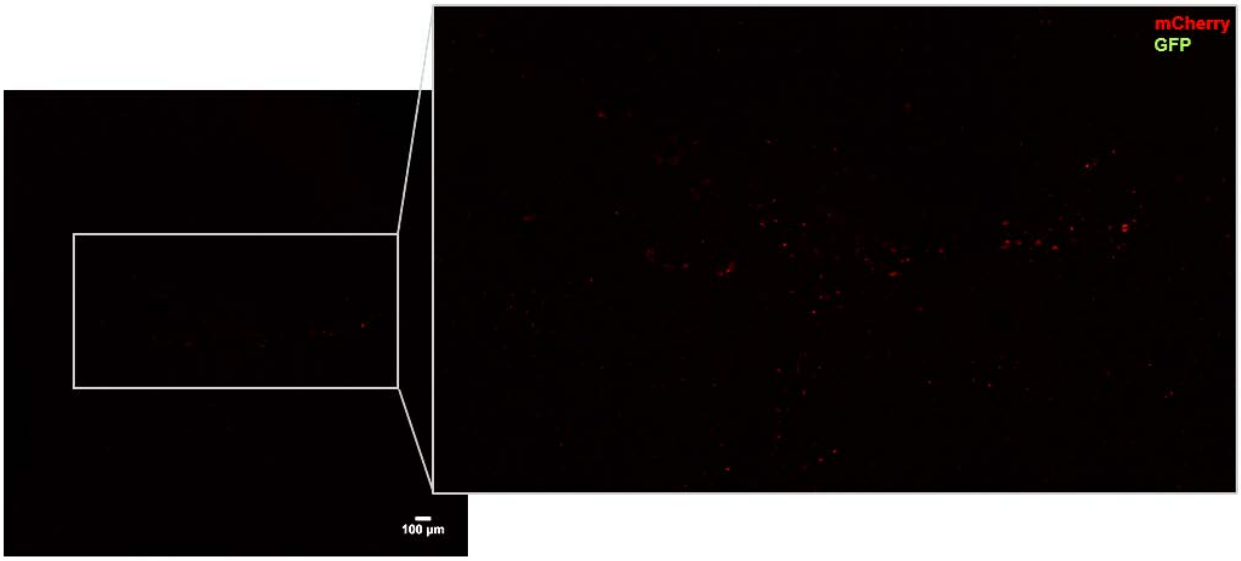

Figure A. 1 Representative image of central IC in DREADDs injected animal (DR01). GFP and mCherry expression are merged in the image. The right insert is the magnified image of the outlined area in the left image. Scale bar on the left image represents 100 µm.

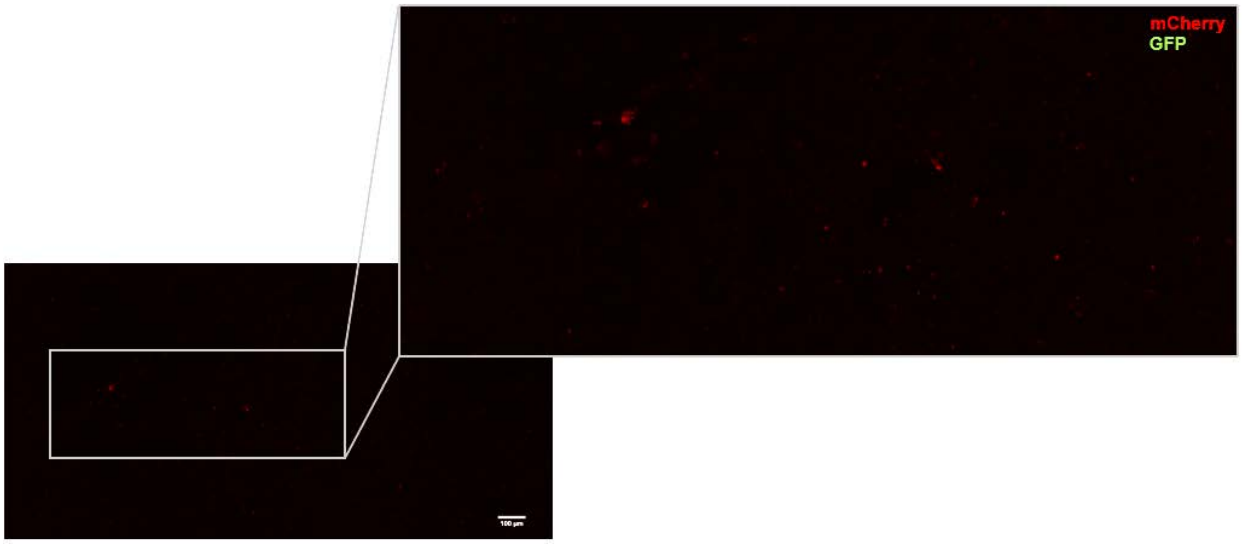

Figure A. 2. Representative image of central IC in DREADDs injected animal (DR02). GFP and mCherry expression are merged in the image. The right insert is the magnified image of the outlined area in the left image. Scale bar on the left image represents 100 µm.

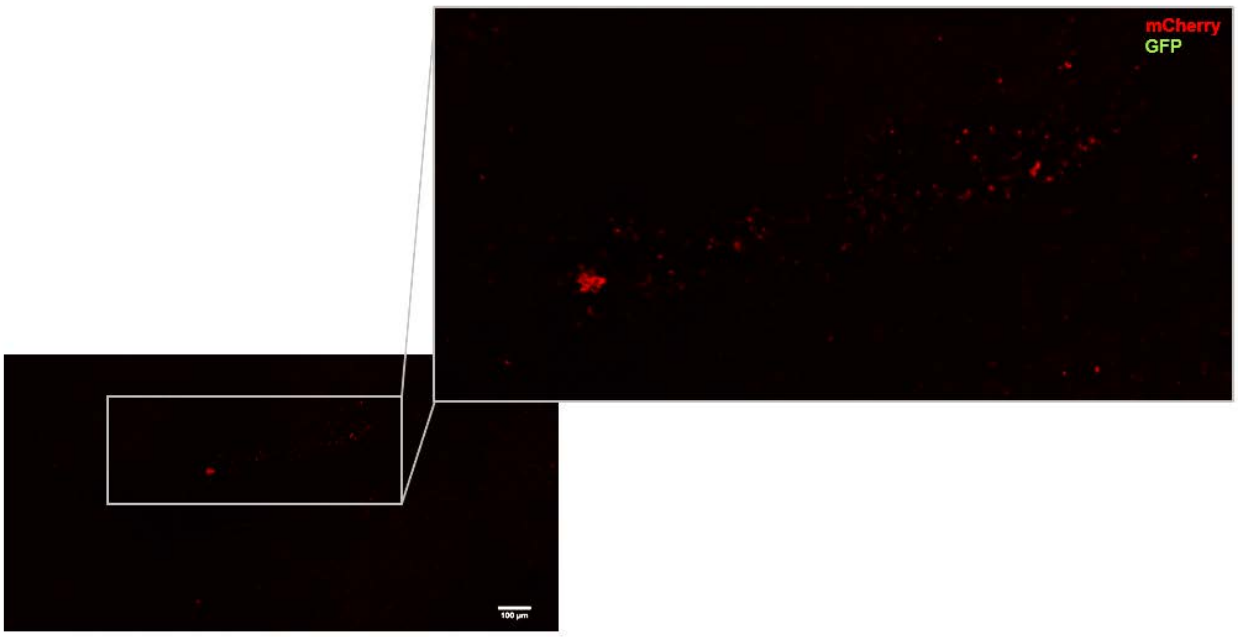

Figure A. 3 Representative image of central IC in DREADDs injected animal (DR04). GFP and mCherry expression are merged in the image. The right insert is the magnified image of the outlined area in the left image. Scale bar on the left image represents 100 µm.

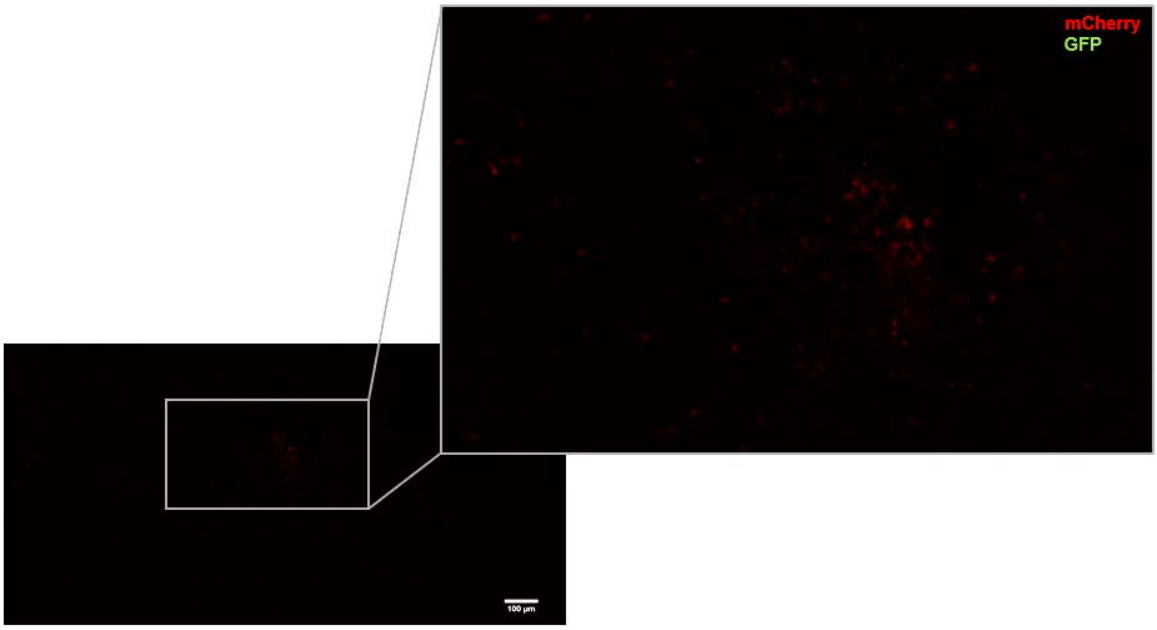

Figure A. 4 Representative image of central IC in DREADDs injected animal (DR05). GFP and mCherry expression are merged in the image. The right insert is the magnified image of the outlined area in the left image. Scale bar on the left image represents 100 µm.

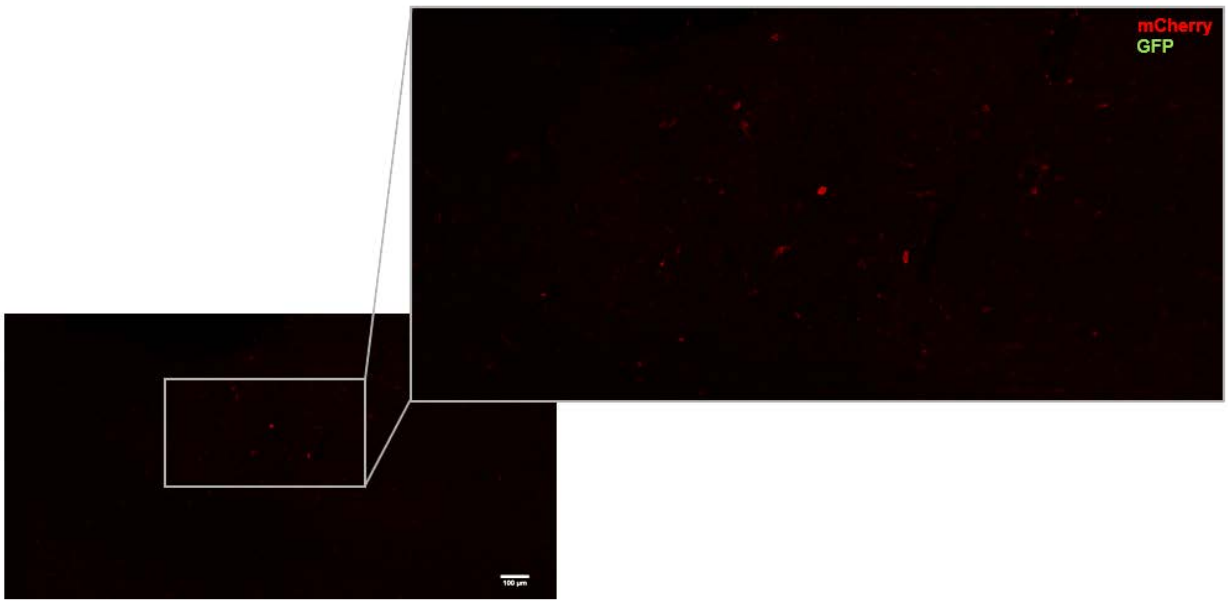

Figure A. 5 Representative image of central IC in DREADDs injected animal (DR06). GFP and mCherry expression are merged in the image. The right insert is the magnified image of the outlined area in the left image. Scale bar on the left image represents 100 μm.

REFERENCES

[1] "Hearing Foundation Of India." [Online]. Available: http://www.hearingfoundation.in/. [Accessed: 30-Jul-2018].

[2] D. Purves, G. J. Augustine, D. Fitzpatrick, W. C. Hall, A.-S. LaMantia, and L. E. White, Eds., "The auditory system," in *Neuroscience*, 5th ed., Sunderland: Sinauer Associates, 2012.

[3] H.-S. Li-Korotky, "Age-Related Hearing Loss: Quality of Care for Quality of Life," *Gerontologist*, vol. 52, no. 2, pp. 265–271, Apr. 2012.

[4] Q. Huang and J. Tang, "Age-related hearing loss or presbycusis," *Eur. Arch. Oto-Rhino-Laryngology*, vol. 267, no. 8, pp. 1179–1191, Aug. 2010.

[5] N. R. Peterson, D. B. Pisoni, and R. T. Miyamoto, "Cochlear implants and spoken language processing abilities: review and assessment of the literature.," *Restor. Neurol. Neurosci.*, vol. 28, no. 2, pp. 237–50, 2010.

[6] J. O. Pickles, "Auditory pathways: anatomy and physiology.," *Handb. Clin. Neurol.*, vol. 129, pp. 3–25, 2015.

[7] V. M. Bajo, F. R. Nodal, D. R. Moore, and A. J. King, "The descending corticocollicular pathway mediates learning-induced auditory plasticity," *Nat. Neurosci.*, vol. 13, no. 2, pp. 253–260, Feb. 2010.

[8] W. Yan and N. Suga, "Corticofugal modulation of the midbrain frequency map in the bat auditory system," *Nat. Neurosci.*, vol. 1, no. 1, pp. 54–58, May 1998.

[9] R. F. Huffman and O. W. Henson, "The descending auditory pathway and acousticomotor systems: connections with the inferior colliculus," *Brain Res. Rev.*, vol. 15, no. 3, pp. 295–323, Sep. 1990.

[10] M. D. Seidman, N. Ahmad, and U. Bai, "Molecular mechanisms of age-related hearing loss.," *Ageing Res. Rev.*, vol. 1, no. 3, pp. 331–43, Jun. 2002.

[11] D. M. Caspary, L. Ling, J. G. Turner, and L. F. Hughes, "Inhibitory neurotransmission, plasticity and aging in the mammalian central auditory system," *J. Exp. Biol.*, vol. 211, no. 11, pp. 1781–1791, Jun. 2008.

[12] T. Ito and D. L. Oliver, “Local and commissural IC neurons make axosomatic inputs on large GABAergic tectothalamic neurons,” *J. Comp. Neurol.*, vol. 522, no. 15, pp. 3539–3554, Oct. 2014.

[13] A. Krishnan, “Human frequency-following responses: representation of steady-state synthetic vowels.,” *Hear. Res.*, vol. 166, no. 1–2, pp. 192–201, Apr. 2002.

[14] S. Kaur, R. Lazar, and R. Metherate, “Intracortical Pathways Determine Breadth of Subthreshold Frequency Receptive Fields in Primary Auditory Cortex,” *J. Neurophysiol.*, vol. 91, no. 6, pp. 2551–2567, Jun. 2004.

[15] B. L. Roth, “DREADDs for Neuroscientists.,” *Neuron*, vol. 89, no. 4, pp. 683–94, Feb. 2016.

[16] K. S. Smith, D. J. Bucci, B. W. Luikart, and S. V Mahler, “DREADDS: Use and application in behavioral neuroscience.,” *Behav. Neurosci.*, vol. 130, no. 2, pp. 137–55, Apr. 2016.

[17] P. D. Whissell, S. Tohyama, and L. J. Martin, “The Use of DREADDs to Deconstruct Behavior,” *Front. Genet.*, vol. 7, p. 70, May 2016.

[18] A. J. Boender, J. W. de Jong, L. Boekhoudt, M. C. M. Luijendijk, G. van der Plasse, and R. A. H. Adan, “Combined Use of the Canine Adenovirus-2 and DREADD-Technology to Activate Specific Neural Pathways In Vivo,” *PLoS One*, vol. 9, no. 4, p. e95392, Apr. 2014.

[19] J.-M. Guettier *et al.*, “A chemical-genetic approach to study G protein regulation of β cell function in vivo,” *Proc. Natl. Acad. Sci.*, vol. 106, no. 45, pp. 19197–19202, Nov. 2009.

[20] G. M. Alexander *et al.*, “Remote Control of Neuronal Activity in Transgenic Mice Expressing Evolved G Protein-Coupled Receptors,” *Neuron*, vol. 63, no. 1, pp. 27–39, Jul. 2009.

[21] J. O.-Y. Yau and G. P. McNally, “Pharmacogenetic excitation of dorsomedial prefrontal cortex restores fear prediction error.,” *J. Neurosci.*, vol. 35, no. 1, pp. 74–83, Jan. 2015.

[22] S. M. Ferguson, P. E. M. Phillips, B. L. Roth, J. Wess, and J. F. Neumaier, “Direct-pathway striatal neurons regulate the retention of decision-making strategies.,” *J. Neurosci.*, vol. 33, no. 28, pp. 11668–76, Jul. 2013.

[23] C. Zhan *et al.*, “Acute and long-term suppression of feeding behavior by POMC neurons in the brainstem and hypothalamus, respectively.,” *J. Neurosci.*, vol. 33, no. 8, pp. 3624–32, Feb. 2013.

[24] N. A. Upright *et al.*, “Behavioral effect of chemogenetic inhibition is directly related to receptor transduction levels in rhesus monkeys,” *bioRxiv*, p. 331694, May 2018.

[25] S. M. Ferguson and J. F. Neumaier, “Using DREADDs to investigate addiction behaviors,” *Curr. Opin. Behav. Sci.*, vol. 2, pp. 69–72, Apr. 2015.

[26] R. L. Lowery and A. K. Majewska, “Intracranial Injection of Adeno-associated Viral Vectors,” *J. Vis. Exp.*, no. 45, pp. e2140–e2140, Nov. 2010.

[27] D. R. Stapells and P. Oates, “Estimation of the pure-tone audiogram by the auditory brainstem response: a review.,” *Audiol. Neurootol.*, vol. 2, no. 5, pp. 257–80, 1997.

[28] J. J. Eggermont, “Development of Auditory Evoked Potentials,” *Acta Otolaryngol.*, vol. 112, no. 2, pp. 197–200, Jan. 1992.

[29] T.-J. Chen and S.-S. Chen, “Generator study of brainstem auditory evoked potentials by a radiofrequency lesion method in rats,” *Exp. Brain Res.*, vol. 85, no. 3, pp. 537–542, Jul. 1991.

[30] H. Guest, K. J. Munro, G. Prendergast, R. E. Millman, and C. J. Plack, “Impaired speech perception in noise with a normal audiogram: No evidence for cochlear synaptopathy and no relation to lifetime noise exposure,” *Hear. Res.*, vol. 364, pp. 142–151, Jul. 2018.

[31] J. Lai, A. L. Sommer, and E. L. Bartlett, “Age-related changes in envelope-following responses at equalized peripheral or central activation,” *Neurobiol. Aging*, vol. 58, pp. 191–200, Oct. 2017.

[32] A. Parthasarathy and E. Bartlett, “Two-channel recording of auditory-evoked potentials to detect age-related deficits in temporal processing.,” *Hear. Res.*, vol. 289, no. 1–2, pp. 52–62, Jul. 2012.

[33] B. Herrmann, A. Parthasarathy, E. X. Han, J. Obleser, and E. L. Bartlett, “Sensitivity of rat inferior colliculus neurons to frequency distributions.,” *J. Neurophysiol.*, vol. 114, no. 5, pp. 2941–54, Nov. 2015.

[34] C. F. Rabang, A. Parthasarathy, Y. Venkataraman, Z. L. Fisher, S. M. Gardner, and E. L. Bartlett, “A computational model of inferior colliculus responses to amplitude modulated sounds in young and aged rats.,” *Front. Neural Circuits*, vol. 6, p. 77, 2012.

[35] Q. Wang and L. Li, “Differences between auditory frequency-following responses and onset responses: Intracranial evidence from rat inferior colliculus,” *Hear. Res.*, vol. 357, pp. 25–32, Jan. 2018.

[36] O. R. Floody and M. P. Kilgard, “Differential reductions in acoustic startle document the discrimination of speech sounds in rats,” *J. Acoust. Soc. Am.*, vol. 122, no. 4, pp. 1884–1887, Oct. 2007.

[37] B. Valsamis and S. Schmid, “Habituation and Prepulse Inhibition of Acoustic Startle in Rodents,” *J. Vis. Exp.*, no. 55, pp. e3446–e3446, Sep. 2011.

[38] J. Lai and E. L. Bartlett, “Age-related decline in behavioral discrimination of amplitude modulation frequencies compared to envelope-following responses,” *bioRxiv*, p. 193268, Sep. 2017.

[39] J. S. Yeomans, D. Bosch, N. Alves, A. Daros, R. J. Ure, and S. Schmid, “BEHAVIORAL NEUROSCIENCE GABA receptors and prepulse inhibition of acoustic startle in mice and rats,” vol. 31, no. March, pp. 2053–2061, 2010.

[40] G. Paxinos and C. Watson, *The rat brain in stereotaxic coordinates*. Elsevier, 2007.

[41] R. Land, A. Burghard, and A. Kral, “The contribution of inferior colliculus activity to the auditory brainstem response (ABR) in mice,” *Hear. Res.*, vol. 341, pp. 109–118, Nov. 2016.

[42] S. V Mahler and G. Aston-Jones, “CNO Evil? Considerations for the Use of DREADDs in Behavioral Neuroscience,” *Neuropsychopharmacology*, vol. 43, no. 5, pp. 934–936, Apr. 2018.

[43] D. F. Manvich *et al.*, “The DREADD agonist clozapine N-oxide (CNO) is reverse-metabolized to clozapine and produces clozapine-like interoceptive stimulus effects in rats and mice,” *Sci. Rep.*, vol. 8, no. 1, p. 3840, Dec. 2018.

[44] J. L. Gomez *et al.*, “Chemogenetics revealed: DREADD occupancy and activation via converted clozapine.,” *Science*, vol. 357, no. 6350, pp. 503–507, Aug. 2017.

[45] C. Zincarelli, S. Soltys, G. Rengo, and J. E. Rabinowitz, “Analysis of AAV Serotypes 1–9 Mediated Gene Expression and Tropism in Mice After Systemic Injection,” *Mol. Ther.*, vol. 16, no. 6, pp. 1073–1080, Jun. 2008.

[46] J. G. Mellott, M. E. Bickford, and B. R. Schofield, “Descending projections from auditory cortex to excitatory and inhibitory cells in the nucleus of the brachium of the inferior colliculus,” *Front. Syst. Neurosci.*, vol. 8, p. 188, Oct. 2014.

[47] H. Nomura *et al.*, “Memory formation and retrieval of neuronal silencing in the auditory cortex.,” *Proc. Natl. Acad. Sci. U. S. A.*, vol. 112, no. 31, pp. 9740–4, Aug. 2015.

[48] J. A. Winer, R. L. Saint Marie, D. T. Larue, and D. L. Oliver, “GABAergic feedforward projections from the inferior colliculus to the medial geniculate body.,” *Proc. Natl. Acad. Sci. U. S. A.*, vol. 93, no. 15, pp. 8005–10, Jul. 1996.

[49] D. Peruzzi, E. Bartlett, P. H. Smith, and D. L. Oliver, “A monosynaptic GABAergic input from the inferior colliculus to the medial geniculate body in rat.,” *J. Neurosci.*, vol. 17, no. 10, pp. 3766–77, May 1997.

[50] T. Ito, D. C. Bishop, and D. L. Oliver, “Two classes of GABAergic neurons in the inferior colliculus.,” *J. Neurosci.*, vol. 29, no. 44, pp. 13860–9, Nov. 2009.

[51] E. Vardy *et al.*, “A New DREADD Facilitates the Multiplexed Chemogenetic Interrogation of Behavior.,” *Neuron*, vol. 86, no. 4, pp. 936–946, May 2015.

[52] J. G. Mellott, N. L. Foster, A. P. Ohl, and B. R. Schofield, “Excitatory and inhibitory projections in parallel pathways from the inferior colliculus to the auditory thalamus.,” *Front. Neuroanat.*, vol. 8, p. 124, 2014.

[53] J. O. Szablowski, B. Lue, A. Lee-Gosselin, D. Malounda, and Mi. G. Shapiro, “Acoustically Targeted Chemogenetics for Noninvasive Control of Neural Circuits,” *bioRxiv*, p. 241406, Jan. 2018.

[54] W. T. Keenan, D. C. Fernandez, L. J. Shumway, H. Zhao, and S. Hattar, “Eye-Drops for Activation of DREADDs,” *Front. Neural Circuits*, vol. 11, p. 93, Nov. 2017.